Table 2
Association between N1 with #10 below and N2 with only #7 clinicopathological variables.

Characteristics	n1 with #10 below 20	n2 only #7 25	*P* value
Age (years)			
Mean	59.3	60.8	0.75
<65/≧65	12/8	17/8	0.58
Sex			
Male/female	7/13	5/20	0.26
Side			
Right/left	7/13	18/7	0.01
pT Factor			
pT1	5	7	0.94
pT2	6	6	
pT3	3	3	
pT4	6	9	
Tumour size (mm)			
Mean	38.8	37.4	0.93
Operation			
Lobectomy	13	10	0.15
Bilobectomy	2	8	
Pneumonectomy	5	7	
PM			
pm0/pm1	14/6	17/8	0.89
Pathological type			
Adenocarcinoma	13	15	0.52
Squamous cell carcinoma	5	7	
Large-cell carcinoma	0	2	
Other	2	1	

had metastasis to the #7 lymph node (Table 1). There were 37 cases (rt:lt = 24:13) with both #10 below and #7 metastasis (double-positive group), while 28 cases (rt:lt = 10:18) were positive for #10 below but negative for #7(only #10 group). There were 29 (rt:lt = 20:9) cases that were negative for #10 below but positive for #7 (only #7 group).

Superior mediastinal lymph node (SML; highest mediastinal nodes, paratracheal nodes, pretracheal nodes, anterior mediastinal nodes, posterior mediastinal nodes, tracheobronchial angle nodes, Botallo's nodes, para-aortic nodes and ascending aortic nodes) metastasis was seen in 43 (rt:lt = 28:15) cases, while 26 (rt:lt = 11:15) cases had #8.9 metastasis.

Patients with N1 disease were subdivided into two groups. Separation was based on the involvement of #10 below ('N1+', $n = 20$) or absence of involvement ('N1−', $n = 46$). Patients with N2 disease were also subdivided into two groups: those with involvement of only the #7 lymph node metastasis ('N2s', $n = 25$) and those with involvement of any other type of the pN2 lymph node ('N2o', $n = 58$). These groups were defined as the SML or the #8.9 positive groups.

3.2. Associations between lymph node-metastasis distribution and clinicopathological variates

Table 2 summarises the associations between 'N1+' and 'N2s'. No significant association was found between the lymph node-metastasis distribution and age, gender, pT factor, tumour size, type of operation, pM factor and pathological type. However, a close association was demonstrated for location, as the N1+ had a significantly higher incidence (13 of 20, 65.0%) in the left lower lobe as compared to the right lower lobe. In contrast, the N2s had a lower incidence (7 of 25, 28.0%) in the left versus the right lobe ($P = 0.01$).

Associations among the double-positive, only #10 and only #7 groups are summarised in Table 3. There was a significantly higher incidence (64.9%, 24/37) of SML metastasis for the double-positive group as compared to only #10 group (14.3%, 4/28) and only #7 group (31.0%, 9/29) ($P < 0.001$).

Table 3
Association between lymph node metastasis and clinicopathological variables.

Characteristics	#10 below positive/#7 negative 28	#10 below negative/#7 positive 29	#10 below positive/#7 positive 37	*P* value
Age (years)				
<65/≧65	18/10	13/16	26/11	0.09
Sex				
Male/female	18/10	22/7	24/13	0.56
Side				
Right/left	10/18	20/9	24/13	0.02
pT Factor				
pT1	6	6	8	1
pT2	10	11	14	
pT3	3	3	3	
pT4	9	9	12	
PM				
pm0/pm1	19/9	21/8	25/12	0.91
Pathological type				
AD/non-AD	19/9	14/15	28/9	0.06
SMD				
Positive/negative	4/24	9/20	24/13	<0.001
#8 or 9 lymph node				
Positive/negative	5/23	6/23	11/26	0.49

AD, adenocarcinoma; SMD, superior mediastinal lymph node.

3.3. Prognosis by type of lymph node involvement

The prognosis of patients with 'N1—', 'N1+', 'N2s' and 'N2o' were evaluated and the 5-year survival rates were 48%, 45%, 40% and 22%, respectively (Fig. 1). Of the four groups, only 'N1—' and 'N2o' exhibited any significant difference ($P < 0.01$). The overall 5-year survival rates for the N2 with #7 only ($n = 25$) and for the other types (SML or #8.9 positive; $n = 58$) were 40% and 22%, respectively, although this difference was not statistically significant ($P = 0.18$) (Fig. 1).

In the TNM sixth edition, the overall 5-year survival rates for the 66 pN1 and 83 pN2cases were 47% and 28%, respectively, and this difference was statistically significant ($P < 0.001$). After the re-organisation of the seventh TNM edition from the seventh edition, the N1+ cases ($n = 20$) were changed to pN2 from their previous pN1 classification, and thus, the overall 5-year survival rates for the 46 pN1 and 103 pN2cases were 48% and 31%, respectively. This difference was statistically significant ($P = 0.001$) (Fig. 2).

The overall 5-year survival rates for the only #10 group, only #7 group and the double-positive group were 50%, 28% and 22%, respectively. Of the three groups, only #10 group versus only #7 group and only #10 group versus double-positive group exhibited significant difference ($P = 0.05$ and 0.02, respectively) (Fig. 3). Although the difference between only #7 group versus double-positive group was not statistically significant ($P = 0.80$) (Fig. 3). The overall survival rates for the SML-negative ($n = 106$) and SML-positive ($n = 43$) cases were 43% and 19%, respectively. This difference was also significant ($P = 0.004$) (Fig. 4).

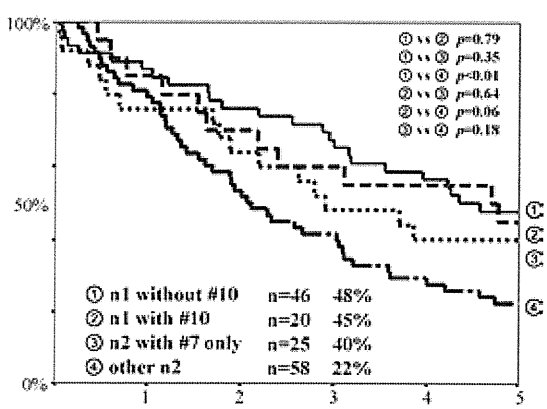

Fig. 1. Survival rates according to #10 below and #7 metastasis.

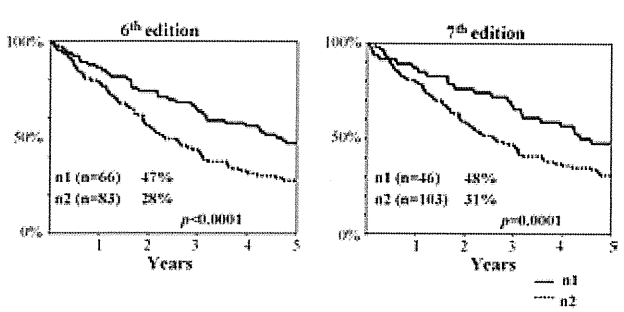

Fig. 2. Survival rates according to 6th and 7th editions of the TNM classification.

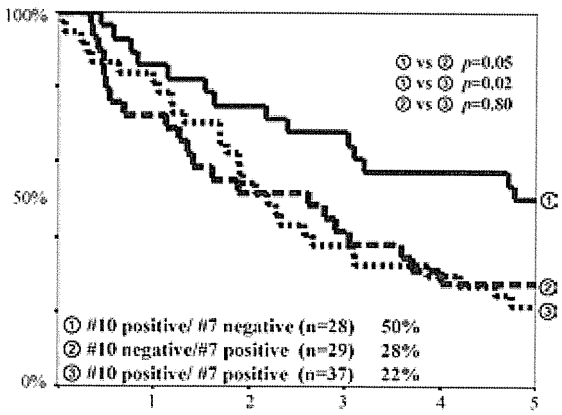

Fig. 3. Survival rates according to #10 and #7 metastasis.

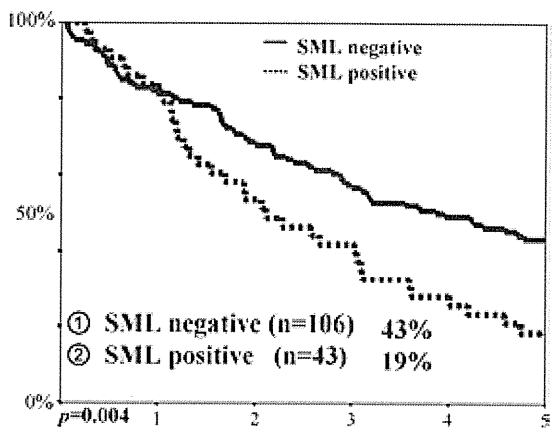

Fig. 4. Survival rates according to SML metastasis.

4. Discussion

The major correction of the seventh TNM classification re-organisation involved the inclusion of the #10 below lymph node in the 'subcarinal zone'. In the current study, we only evaluated the prognoses of N1 with #10 below and N2 with #7, which were found to have 5-year survival rates of 45% and 40%, respectively (Fig. 1). This difference was not statistically significant. The re-organisation of the sixth to the seventh TNM edition resulted in the N1 with #10 below cases being changed into pN2 from pN1. Therefore, the overall 5-year survival rates for the 46 pN1 and 103 pN2 cases that were classified according to the TNM seventh edition were 48% and 31%, respectively, and this difference was statistically significant ($P = 0.001$) (Fig. 2). The changes that were implemented in the seventh TNM edition not only were correct but also quite understandable, as the N1+ cases are indeed a group that has a poor prognosis within pN1. Other reports have also shown that the prognoses for these groups to be identical. Asamura et al. [14] reported that N1 with #10 involvement and the single-station N2 survival curves could be superimposed. In addition, the 5-year survival rates were 54% and 53%, respectively. Rea et al. [15] also reported similar results, although the 5-year survival rates were 31% and 18%, respectively, which were not significant. Others authors [16—19] have reported significantly worse survival

rates for extra-lobar N1 disease as compared to intra-lobar N1 disease.

In the current study, the overall 5-year survival rates for SML-negative ($n = 106$) and SML-positive ($n = 43$) cases were 43% and 19%, respectively, a difference that was statistically significant ($P = 0.004$) (Fig. 4). Okada et al. [20] observed that the patients with lower mediastinal metastasis had a significantly better prognosis than those with upper mediastinal metastasis, with 5-year survival rates of 24.8% and 0%, respectively, a difference that was statistically significant ($P = 0.0446$).

The most important finding of our current study concerned the prevalence of SML metastasis that occurred from the #10 positive and #7 negative and from the #7-positive cases. There was a significantly higher incidence (64.9%, 24/37) of SML metastasis for the double-positive group as compared to only #10 group (14.3%, 4/28) and only #7 group (31.0%, 9/29) ($P < 0.001$) (Table 3). From these results, the prognostic differences were calculated, with the overall 5-year survival rates for the only #10 group, only #7 group and the double-positive group were 50%, 28% and 22%, respectively ($P = 0.05$) (Fig. 3). The results suggest that the most important problem is the prevalence of SML metastasis and the integration of the #10 below and #7 lymph node within the 'subcarinal zone'.

An association was found between the #10 below and the #7 metastasis distribution. Our results demonstrated that there was a close relationship with the location that was involved. There was a significantly higher incidence of N1+ (13 of 20, 65.0%) in the left lower lobe as compared to the right lower lobe while the N2s had a lower incidence (7 of 25, 28.0%) in the left versus the right lobe ($P = 0.01$) (Table 2). This is the first time that this has been reported and the reason for this might be related to differences that exist for the anatomical length of the bilateral #10 below.

In conclusion, when examining survival rates for cases without SML metastasis, no problems are encountered when the #10 and #7 cases are bundled. However, as compared to #10 metastasis, #7 metastasis is a prognostic risk factor for highly advanced SML metastasis and poor patient outcome. Therefore, since #10 below and #7 provide different types of diagnostic information, they may not be bundled together during patient evaluations.

Acknowledgements

We thank Yukitoshi Satoh, Department of Thoracic Surgery, Kitazato University, Sagamihara, Kanagawa, Japan, for his critical review of the manuscript.

References

[1] Mountain CF. A new international staging system for lung cancer. Chest 1986;89:225–33.
[2] Mountain CF. Revision in the international system for staging lung cancer. Chest 1997;111:1710–7.
[3] Rusch VW, Crowley J, Giroux DJ, Goldstraw P, Im JG, Tsuboi M, Tsuchiya R, Vansteenkiste J. The IASLC Lung Cancer Staging Project: proposals for the revision of the N descriptors in the forthcoming seventh edition of the TNM Classification for Lung Cancer. J Thorac Oncol 2007;2:603–12.
[4] Rusch VW, Asamura H, Watanabe H, Giroux DJ, Rami-Porta R, Goldstraw P. The IASLC Lung Cancer Staging Project: a proposal for a New International Lymph Node Map in the Forthcoming Seventh Edition of the TNM classification for lung cancer. J Thorac Oncol 2009;4:568–77.
[5] Naruke T, Suemasu K, Ishikawa S. Lymph node mapping and curability at various levels of metastasis in resected lung cancer. J Thorac Cardiovasc Surg 1978;76:832–9.
[6] The Japan Lung Cancer Society. Classification of Lung Cancer, 1st English Ed. Tokyo: Kanehara & Co.; 2000.
[7] Mountain CF, Dresler CM. Regional lymph node classification for lung cancer staging. Chest 1997;111:1718–23.
[8] Jett J, Feins R, Kvale P. Pretreatment evaluation of non-small cell lung cancer. Am J Respir Crit Care Med 1997;156:320–32.
[9] Tisi GM, Friedman PJ, Peters RM. Clinical staging of primary lung cancer. Am Rev Respir Dis 1983;127:659–64.
[10] Japan Lung Cancer Society, editor. General rule for clinical and pathologic record of lung cancer. 6th ed., Tokyo: Kanahara; 2003:98 [in Japanese].
[11] International Union Against Cancer. TNM classification of malignant tumors. 5th ed., New York: Wiley-Liss; 1997:93–7.
[12] Naruke T, Tsuchiya R, Kondo H, Nakayama H, Asamura H. Lymph node sampling in lung cancer: how should it be done? Eur J Cardiothorac Surg 1999;16:17–24.
[13] World Health Organization. The World Health Organization histological typing of lung tumours. Geneva: World Health Organization; 1999:21–4.
[14] Asamura H, Suzuki K, Kondo H, Tsuchiya R. Where is the boundary between N1 and N2 stations in lung cancer. Ann Thorac Surg 2000;70:1839–46.
[15] Rea F, Marulli G, Callegaro D, Zuin A, Gobbi T, Loy M, Sartori F. Prognostic significance of main bronchial lymph nodes involvement in non-small cell lung carcinoma: N1 or N2? Lung Cancer 2004;45:215–20.
[16] Yano T, Yokoyama H, Inoue T, Asoh H, Tayama K, Ichinose Y. Surgical results and prognostic factors of pathologic N1 disease in non-small cell carcinoma of the lung. Significance of N1 level: lobar or hilar nodes. J Thorac Cardiovasc Surg 1994;107:1398–402.
[17] Ueda K, Kaneda Y, Saeki K, Fujita N, Zempo N, Esato K. Hilar lymph nodes in N2 disease: survival analysis of patients with non-small cell lung cancer and regional lymph node metastasis. Surg Today 2002;32:300–4.
[18] Tanaka F, Yanagihara K, Otake Y, Yamada T, Shoji T, Miyahara R, Inui K, Wada H. Prognostic factors in patients with resected pathologic (p-) T1-2N1M0 non-small cell lung cancer (NSCLC). Eur J Cardiothorac Surg 2001;19:555–61.
[19] Van Velzen E, Snijder RJ, Brutel de la Riviere A, Elbers HR, Van den Bosch JM. Lymph node type as a prognostic factor for survival in T2 N1 M0 non-small cell lung carcinoma. Ann Thorac Surg 1997;63:1436–40.
[20] Okada M, Sakamoto T, Yuki T, Mimura T, Nitanda H, Miyoshi K, Tsubota N. Border between N1 and N2 stations in lung carcinoma: lessons from lymph node metastatic patterns of lower lobe tumors. J Thorac Cardiovasc Surg 2005;129:825–30.

Cancer Research

Intrinsic Cooperation between $p16^{INK4a}$ and $p21^{Waf1/Cip1}$ in the Onset of Cellular Senescence and Tumor Suppression *In vivo*

Shinji Takeuchi[1,4,6], Akiko Takahashi[1], Noriko Motoi[2], Shin Yoshimoto[1], Tomoko Tajima[1,3], Kimi Yamakoshi[1], Atsushi Hirao[5], Shigeru Yanagi[3], Kiyoko Fukami[3], Yuichi Ishikawa[2], Saburo Sone[6], Eiji Hara[1], and Naoko Ohtani[1]

Abstract

Although the $p16^{INK4a}$ and $p21^{Waf1/Cip1}$ cyclin-dependent kinase (CDK) inhibitors are known to play key roles in cellular senescence *in vitro*, their roles in senescence remain rather poorly understood *in vivo*. This situation is partly due to the possibility of compensatory effect(s) between $p16^{INK4a}$ and $p21^{Waf1/Cip1}$ or to the upregulation of functionally related CDK inhibitors. To directly address the cooperative roles of $p16^{INK4a}$ and $p21^{Waf1/Cip1}$ in senescence *in vivo*, we generated a mouse line simply lacking both $p16^{INK4a}$ and $p21^{Waf1/Cip1}$ genes [double-knockout (DKO)]. Mouse embryonic fibroblasts (MEF) derived from DKO mice displayed no evidence of cellular senescence when cultured serially *in vitro*. Moreover, DKO MEFs readily escaped Ras-induced senescence and overrode contact inhibition in culture. This was not the case in MEFs lacking either $p16^{INK4a}$ or $p21^{Waf1/Cip1}$, indicating that $p16^{INK4a}$ and $p21^{Waf1/Cip1}$ play cooperative roles in cellular senescence and contact inhibition *in vitro*. Notably, we found the DKO mice to be extremely susceptible to 7,12-dimethylbenz (*a*)anthracene/12-*O*-tetradecanoylphorbol-13-acetate–induced skin carcinogenesis that involves oncogenic mutation of the *H-ras* gene. Mechanistic investigations suggested that the high incidence of cancer in DKO mice likely reflected a cooperative effect of increased benign skin tumor formation caused by $p21^{Waf1/Cip1}$ loss, with increased malignant conversion of benign skin tumors caused by $p16^{INK4a}$ loss. Our findings establish an intrinsic cooperation between $p16^{INK4a}$ and $p21^{Waf1/Cip1}$ in the onset of cellular senescence and tumor suppression *in vivo*. *Cancer Res; 70(22); 9381–90. ©2010 AACR.*

Introduction

The $p16^{INK4a}$ and $p21^{Waf1/Cip1}$ cyclin-dependent kinase (CDK) inhibitors are known to play key roles in the onset of cellular senescence, a state of permanent cell cycle arrest in culture (1–6). The simultaneous induction of $p21^{Waf1/Cip1}$ and $p16^{Ink4a}$ expression cooperatively blocks the activation of both cyclin D kinase (CDK4/6) and cyclin E kinase (CDK2), allowing the accumulation of the dephosphorylated form of the retinoblastoma tumor suppressor protein (pRb) and thereby causing permanent cell cycle arrest (7–10). It has become apparent that cellular senescence can be induced by a variety of potentially oncogenic stimuli, such as telomere shortening, DNA damage, oxidative stress, or oncogene expression (11–14), suggesting that cellular senescence is likely to act as a tumor suppression mechanism *in vivo* (15, 16). Although the roles of $p16^{Ink4a}$ and $p21^{Waf1/Cip1}$ in cellular senescence are well documented in various cell culture studies, the *in vivo* roles of these CDK inhibitors are poorly understood (17). For example, mice lacking $p16^{INK4a}$ (18, 19) or $p21^{Waf1/Cip1}$ (20–22) exhibit only a little predisposition to spontaneous tumor formation. These observations raise the question of whether the results seen in cell culture studies truly reflect the physiologic roles of these CDK inhibitors *in vivo*. However, it is also possible that these weak phenotypes could be due to functional compensatory effect(s) between $p16^{Ink4a}$ and $p21^{Waf1/Cip1}$.

To directly address the cooperative roles of $p16^{INK4a}$ and $p21^{Waf1/Cip1}$ *in vivo*, we generated a compound mouse line simply lacking both of the $p16^{INK4a}$ and $p21^{Waf1/Cip1}$ genes [double-knockout (DKO) mouse] on a C57BL/6 background, which is known to be carcinogenesis resistant (23–25), and evaluated the roles of these two critical senescence inducers *in vitro* and *in vivo*. Intriguingly, DKO mice are significantly more susceptible to chemical carcinogenesis compared with mice lacking either $p16^{INK4a}$ or $p21^{Waf1/Cip1}$ alone. Moreover, mouse embryonic fibroblasts (MEF) derived from DKO mice

Authors' Affiliations: Divisons of [1]Cancer Biology and [2]Pathology, The Cancer Institute of Japanese Foundation for Cancer Research (JFCR); [3]School of Life Science, Tokyo University of Pharmacy and Life Sciences, Tokyo, Japan; Divisions of [4]Medical Oncology and [5]Molecular Genetics, Cancer Research Institute, Kanazawa University, Kanazawa, Japan; and [6]Institute of Health Biosciences, University of Tokushima, Tokushima, Japan

Note: Supplementary data for this article are available at Cancer Research Online (http://cancerres.aacrjournals.org/).

Corresponding Author: Naoko Ohtani, Division of Cancer Biology, The Cancer Institute of Japanese Foundation for Cancer Research (JFCR), Tokyo 135-8550, Japan. Phone: 81-3-3570-0605; Fax: 81-3-3570-0457; E-mail: naoko.ohtani@jfcr.or.jp.

doi: 10.1158/0008-5472.CAN-10-0801

are resistant to the onset and the maintenance of cellular senescence in culture. These results indicate that $p16^{INK4a}$ plays a critical role in cooperating with $p21^{Waf1/Cip1}$ in tumor suppression *in vivo*.

Materials and Methods

Generation of $p16^{-/-};p21^{-/-}$ mice

$p16^{-/-}$ mice (C57BL/6) were kindly provided by N.E. Sharpless (University of North Carolina Lineberger Comprehensive Cancer Center, Chapel Hill, NC; ref. 19). *$p21^{-/-}$* mice (C57BL/6) were kindly provided by P. Leder (Harvard Medical School, Boston, MA; ref. 20). *$p16^{-/-};p21^{-/-}$* DKO mice were generated by crossing *$p16^{-/-}$* mice and *$p21^{-/-}$* mice. All animals were cared for by using protocols approved by the Committee for the Use and Care of Experimental Animals of the Japanese Foundation for Cancer Research.

Cell culture

MEFs were generated from E13.5 embryos of wild-type, *$p16^{-/-}$*, *$p21^{-/-}$*, or *$p16^{-/-};p21^{-/-}$* DKO mice as previously described (26). MEFs were grown in DMEM supplemented with 10% fetal bovine serum in 3% O_2/5% CO_2 for 2 days, harvested, viably frozen, and labeled as passage 0. Serial 3T3 cultivation was done as described (27). Cells were counted in triplicate. The number of cells present on the third day (N3) was divided by the initial cell number (N0 = 3×10^5) and plotted as growth rate (N3/N0; Supplementary Fig. S1). The increase in the population doubling level (ΔPDL) was calculated according to the following formula: ΔPDL = log (Nf/N0)/log 2, where N0 is the initial number of cells (3×10^5) and Nf is the final number of cells.

Western blot analysis

Proteins (40 μg) were analyzed by Western blotting, as previously described (6). The primary antibodies used were $p16^{INK4a}$ (11104 IBL), $p21^{Waf1/Cip1}$ (sc-6246, Santa Cruz Biotechnology, Inc.), $p15^{INK4b}$ (sc-613, Santa Cruz Biotechnology), p53 (1C12, Cell Signaling), $p19^{Arf}$ [ab80 (Abcam) or sc-32748 (Santa Cruz Biotechnology)], H-Ras (sc-29, Santa Cruz Biotechnology), pRb (554136, BD Pharmingen), β-actin (AC-74, Sigma-Aldrich), and α-tublin (DM-1A, Sigma-Aldrich). Secondary antibodies were detected by enhanced chemiluminescence (Amersham).

Retrovirus infection and focus formation assay

Retroviral gene transfer was done by transient transfection of the LinxE ecotropic packaging cells with a pBabe-puro vector and the vector containing the human H-rasV12 oncogene, as previously described (6). Forty-eight hours after transfection, the retrovirus-containing medium was collected, filtered, supplemented with 8 μg/mL polybrene (Sigma), and used for multiple infection (twice a day for 2 days) into early-passage MEFs (P0–P1) growing in 3% O_2/5% CO_2. Infected cell populations were selected for 5 days in the presence of 1 μg/mL puromycin. For foci formation assays, 1.7×10^4 puromycin-selected immortalized cells were seeded into 6-cm-diameter dishes. Cells were maintained for 15 days in a 3% O_2/5% CO_2 culture environment, and the medium was changed twice a week until the cells were photographed and counted.

Senescence-associated β-galactosidase assay

Senescence-associated β-galactosidase assay was done as described previously (28).

Analysis of intracellular reactive oxygen species

To assess the generation of intracellular levels of reactive oxygen species (ROS), cells were incubated with 20 μmol/L 2′,7′-dichlorofluorescein diacetate (Calbiochem) for 20 minutes at 37°C. The peak excitation wavelength for oxidized 2′,7′-dichlorofluorescein was 488 nm and the emission wavelength was 525 nm as described previously (6).

Chemically induced skin tumor formation

The chemically induced skin tumor formation analysis was done as described previously (29). Briefly, mice of the wild-type, p16-KO, p21-KO, or DKO genotypes in the resting phase of the hair cycle (8 weeks old) were shaved and treated with 100 μg of 7,12-dimethylbenz(*a*)anthracene (DMBA) in 100 μL of acetone. One week after DMBA treatment, mice were subsequently treated twice a week with 12.5 μg of 12-*O*-tetradecanoylphorbol-13-acetate (TPA) in 100 μL of acetone for 20 weeks. Tumors developed in mice were analyzed for histology at 30 weeks after DMBA treatment.

Histologic analysis

Tissues were fixed in 10% buffered formalin, progressively dehydrated through gradients of alcohol, and embedded in paraffin. Samples were sectioned on a microtome at 4-μm thickness, deparaffinized in xylene, rehydrated, and then stained with H&E for histologic analysis.

Results

$p16^{INK4a};p21^{Waf1/Cip1}$ DKO MEFs proliferate without any induction of cellular senescence by serial passaging

Compound mice lacking both *$p16^{INK4a}$* and *$p21^{Waf1/Cip1}$* on a C57BL/6 background (DKO mice) are fertile and born normally in the expected Mendelian ratio. MEFs derived from wild-type mice, *$p16^{INK4a}$* knockout (p16-KO) mice, *$p21^{Waf1/Cip1}$* knockout (p21-KO) mice, and DKO mice were subjected to serial passage using the 3T3 protocol under standard culture conditions, which included atmospheric (20%) oxygen. Consistent with previous reports, p16-KO MEFs underwent cellular senescence in a kinetic pattern similar to that of wild-type MEFs (Fig. 1A; Supplementary Fig. S1A and C; refs. 18, 19). The level of $p15^{INK4b}$ expression was remarkably increased and the $p21^{Waf1/Cip1}$ level remained high in senescent p16-KO MEFs, implying that a compensatory network among the CDK inhibitors indeed exists as previously suggested (refs. 30–33; Fig. 1C, lanes 1–4 and 10–13). p21-KO MEFs proliferated without detectable senescence growth arrest, although they exhibited a slight reduction in proliferation rate at passage 4, as previously reported (ref. 26; Fig. 1A; Supplementary Fig. S1A

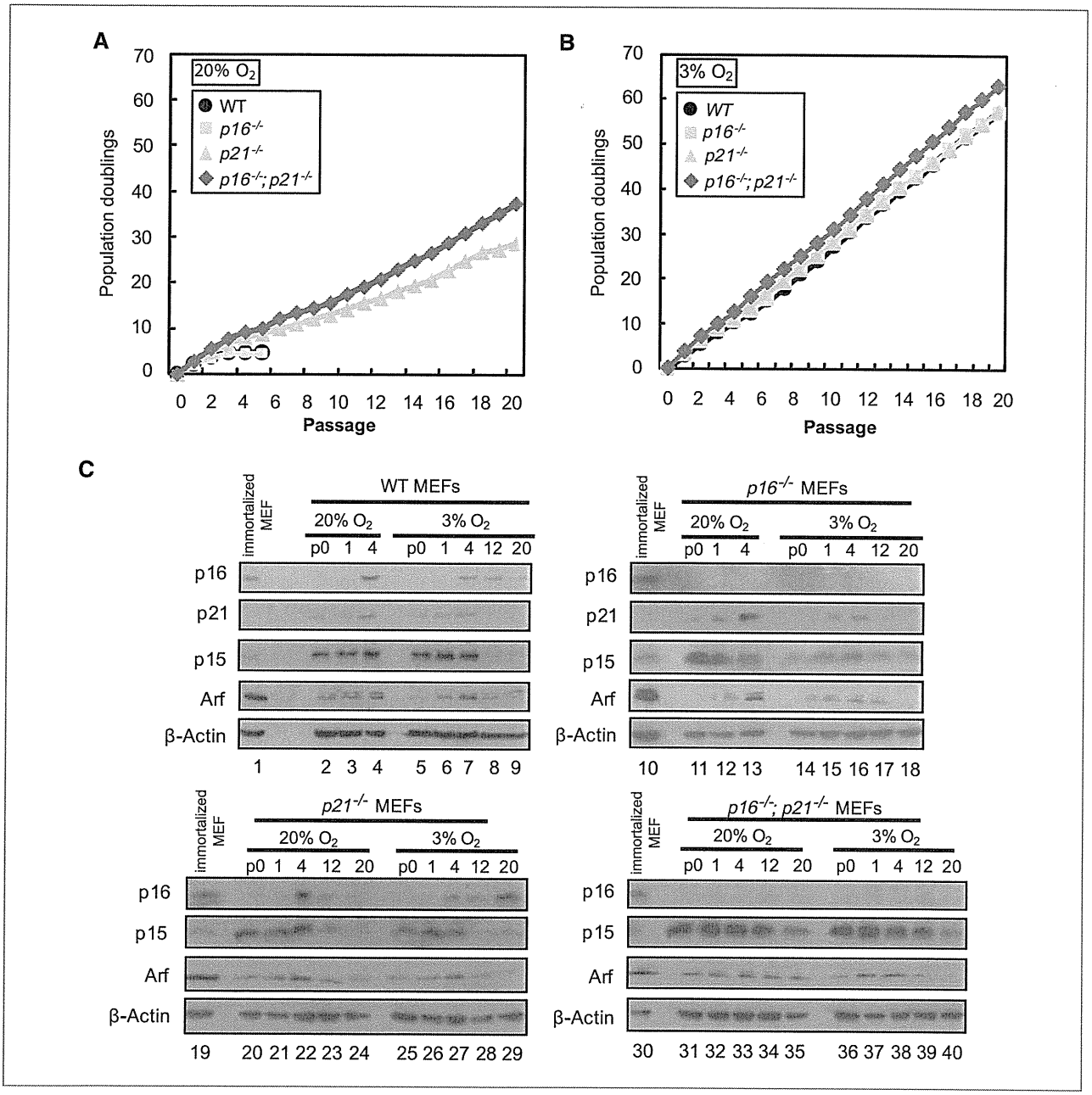

Figure 1. Serial 3T3 cultivation of primary MEFs of different genotypes. A and B, MEFs derived from wild-type (WT), p16-KO, p21-KO, and DKO mice were cultivated according to the 3T3 protocol. The graphs represent the accumulated population doublings at every passage (A, in 20% oxygen; B, in 3% oxygen). The means ± SD of triplicate experiments are shown. C, protein levels of the cell cycle inhibitors $p16^{INK4a}$, $p21^{Waf1/Cip1}$, $p15^{INK4b}$, and $p19^{Arf}$. Note that passage 20 of the wild-type and p16-KO MEFs in 20% oxygen culture could not be analyzed because a very long period of time was required to generate an immortalized culture. To compare the levels of proteins across the gels, the same sample (immortalized MEFs) was loaded on every gel (lanes 1, 10, 19, and 30). β-Actin was used as a loading control. Representative data of two independent experiments are shown. Uncropped images are shown in Supplementary Data.

and C). Interestingly, MEFs lacking both $p16^{INK4a}$ and $p21^{Waf1/Cip1}$ (DKO MEFs) grew slightly but consistently better than p21-KO MEFs, suggesting that $p16^{INK4a}$ also plays a role, at least to some extent, in the cellular senescence provoked by the serial passage of MEFs (Fig. 1A; Supplementary Fig. S1A).

Because primary MEFs have been shown to be exquisitely sensitive to oxidative stress in culture (34), we next cultured these MEFs with 3% oxygen, which is known to be similar to the physiologic oxygen condition *in vivo* (34). In contrast to the result with the 20% oxygen condition, we were unable to see any significant difference in the cell proliferation rate between wild-type MEFs and MEFs lacking the $p16^{INK4a}$ or $p21^{Waf1/Cip1}$ gene (Fig. 1B; Supplementary Fig. S1B and D), although the DKO MEFs proliferated

slightly better than the MEFs of other types (Fig. 1B; Supplementary Fig. S1B). As seen in the 20% oxygen condition, the level of $p15^{INK4b}$ expression, but not the expression of the other $p16^{INK4a}$ family members (data not shown), was substantially increased in both p16-KO MEFs and DKO MEFs under the 3% oxygen condition (Fig. 1C, lanes 1–18 and 30–40), suggesting that $p15^{INK4b}$ may play a compensatory role in the absence of $p16^{INK4a}$ regardless of the oxygen conditions *in vitro*, although this level of $p15^{INK4b}$ expression does not seem to be high enough to block cell proliferation (Fig. 1B; Supplementary Fig. S1B). Furthermore, because the *p19*^{Arf} gene shares a locus with *p16*^{INK4a} and is also implicated in tumor suppression (35, 36), we examined the level of $p19^{Arf}$ in these MEFs. However, we did not see any substantial difference in $p19^{Arf}$ expression in MEFs lacking the *p16*^{INK4a} and/or *p21*$^{Waf1/Cip1}$ gene compared with wild-type MEFs (Fig. 1C).

DKO MEFs expressing oncogenic Ras escape contact inhibition and form foci

Because cellular senescence can also be induced by activated *ras* oncogene expression, we next asked if the status of the *p16*^{INK4a} and/or *p21*$^{Waf1/Cip1}$ gene affects Ras-induced senescence under physiologic (3%) oxygen conditions. In contrast to passage-induced senescence, MEFs of all the genotypes exhibited features of cellular senescence, including cell cycle arrest, a flat and enlarged morphology, and the accumulation of the dephosphorylated form of pRb within 10 days of infection with retrovirus encoding oncogenic Ras (Fig. 2). Notably, increased expression of $p15^{INK4b}$ as well as p53 and $p19^{Arf}$ upregulation was observed in Ras-induced senescence (Fig. 2D). The depletion of $p15^{INK4b}$ by small interference RNA abrogated the appearance of senescence markers in Ras-infected DKO MEFs (Supplementary Fig. S2). It is therefore likely that the upregulation of $p15^{INK4b}$ expression plays an important role, at least partly, in oncogenic Ras–induced senescence in DKO MEFs. However, although the levels of senescence-associated β-galactosidase activity (Fig. 2B) and the intracellular levels of ROS (Fig. 2C), which are markers of cellular senescence, were increased in DKO MEFs, the level of induction was less evident compared with the MEFs of other genotypes. These results raise the possibility that $p16^{INK4a}$ and $p21^{Waf1/Cip1}$ are both required for the full induction of oncogenic Ras–induced senescence in culture. Indeed, DKO MEFs expressing oncogenic Ras readily escaped the senescent state and reinitiated proliferation more rapidly than the MEFs of other genotypes under the 3% oxygen condition (Fig. 3A). Note that the saturation density of the DKO MEFs expressing oncogenic Ras was remarkably higher than that of the other cell types (Fig. 3B). Interestingly, significant numbers of foci were also observed in the confluent culture of the DKO MEFs expressing oncogenic Ras, but not the MEFs of other genotypes, under the 3% oxygen condition (Fig. 3C). Taken together, these results suggest that oncogenic Ras expression, in conjunction with the loss of $p16^{INK4a}$ and $p21^{Waf1/Cip1}$, may have potential to counteract the pathway involved in contact inhibition in cultured MEFs.

DKO mice are extremely susceptible to DMBA/TPA–induced skin cancer

To explore the role of $p16^{INK4a}$ and $p21^{Waf1/Cip1}$ in oncogenic Ras expression in a more physiologic setting, wild-type, p16-KO, p21-KO, and DKO mice were subjected to a conventional chemically induced skin carcinogenesis protocol, with a single dose of DMBA followed by biweekly treatment of TPA for 20 weeks. Because this protocol is known to cause an oncogenic mutation in the endogenous *H-ras* gene, it seemed to be an ideal system for studying the physiologic response to oncogenic Ras expression in living animals (37). In p16-KO mice, the frequency of benign skin papilloma formation was not increased, and the maximum number of papillomas was 6.8 per mouse on average, whereas 6.0 papillomas developed in wild-type mice (Fig. 4A and B). Interestingly, however, 23.08% of the p16-KO mice developed at least one malignant skin tumor (Fig. 4B; Table 1), whereas 5.56% of the wild-type mice developed skin cancer (Fig. 4A; Table 1) at 30 weeks after DMBA treatment. Note that a malignant tumor that appeared in the wild-type mice was carcinoma *in situ*, whereas two thirds of the malignant tumors in the p16-KO mice were more aggressive and invasive cancers (Table 1). The malignant conversion ratio from benign papillomas in p16-KO mice was approximately five times higher than that in wild-type mice (0.93% in wild-type mice versus 4.55% in p16-KO mice; see Table 1), indicating that $p16^{INK4a}$ plays a role in preventing the malignant conversion of benign skin tumors, but not benign skin tumor formation itself, at least in this setting. This is consistent with the observation that $p16^{INK4a}$ expression is upregulated in the late stage (30 weeks after DMBA treatment), but not in the early stage (10 weeks after DMBA treatment), of DMBA/TPA–induced skin papillomas (Supplementary Fig. S3; ref. 29). In addition, the level of $p19^{Arf}$ expression was also increased in the late papillomas (Supplementary Fig. S3), as seen in Ras-induced senescence in cultured MEFs (Fig. 2D). These results suggest that the upregulation of $p19^{Arf}$, at least in part, contributes to the induction of Ras-induced senescence *in vitro* and *in vivo* in mice.

In stark contrast with p16-KO mice, the frequency of benign skin papilloma formation was strikingly increased in p21-KO mice (the maximum number was 12.5 papillomas per mouse; Fig. 4C). However, surprisingly, the malignant conversion rate to advanced cancers was not increased in these p21-KO mice (1.23%) at 30 weeks after DMBA treatment in this setting (Table 1). These results are consistent with the previous observation by Weinberg and colleagues (38), but not with the report by Topley and colleagues (39). However, because each group used different protocols and mouse strains, these seemingly contradictory data are, at least partly, due to the differences in the experimental conditions between our study and the study of Topley and colleagues (39). Nevertheless, a substantial level of $p21^{Waf1/Cip1}$ expression, but not $p16^{INK4a}$ expression, was induced in the early stage of the benign skin papillomas (10 weeks after DMBA treatment; Supplementary Fig. S3). These data imply that a major role of $p21^{Waf1/Cip1}$ is likely to be preventing benign skin papilloma formation rather than the

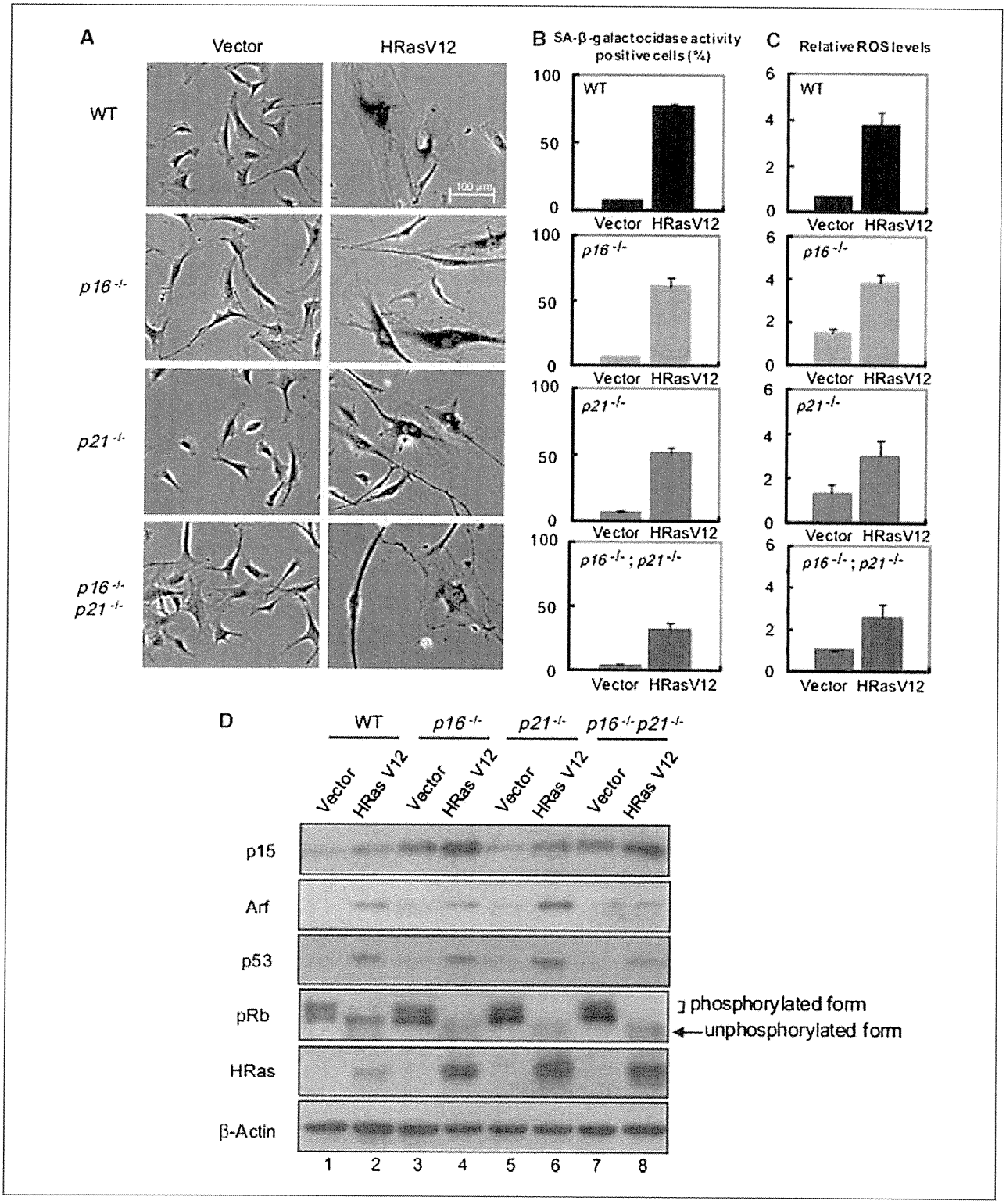

Figure 2. Induction of oncogene-induced cellular senescence by retrovirally transduced oncogenic Ras in wild-type, p16-KO, p21-KO, and DKO MEFs. MEFs of the indicated genotypes were infected with control retrovirus or retrovirus encoding oncogenic Ras, and a series of experiments were performed a week after infection. A, representative photographs of cells; B, percentage of senescence-associated β-galactosidase (SA-β-gal) positive MEFs; C, relative ROS levels. Columns, mean of three independent experiments; bars, SD. D, protein levels of $p15^{INK4b}$, $p19^{Arf}$, p53, Rb, and H-Ras in MEFs infected with retrovirus encoding oncogenic Ras (H-RasV12) or control empty vector (Vector). β-Actin was used as a loading control. Representative data of two independent experiments are shown. Uncropped images are shown in Supplementary Data.

malignant conversion of benign skin tumors, at least in this setting, although it is also possible that $p21^{Waf1/Cip1}$ may have the ability to block progression to higher-grade benign papillomas.

It is interesting that the frequencies of both the benign papilloma formation (the maximum number was 16.0 papillomas per mouse) and the incidence of cancer-bearing mice were dramatically enhanced when DKO mice were subjected to the DMBA/TPA–induced skin carcinogenesis protocol (Fig. 4D; Table 1). By 30 weeks after the DMBA/TPA treatment, 84.21% of the DKO mice developed at least one carcinoma (Fig. 4D; Table 1). Notably, however, the malignant

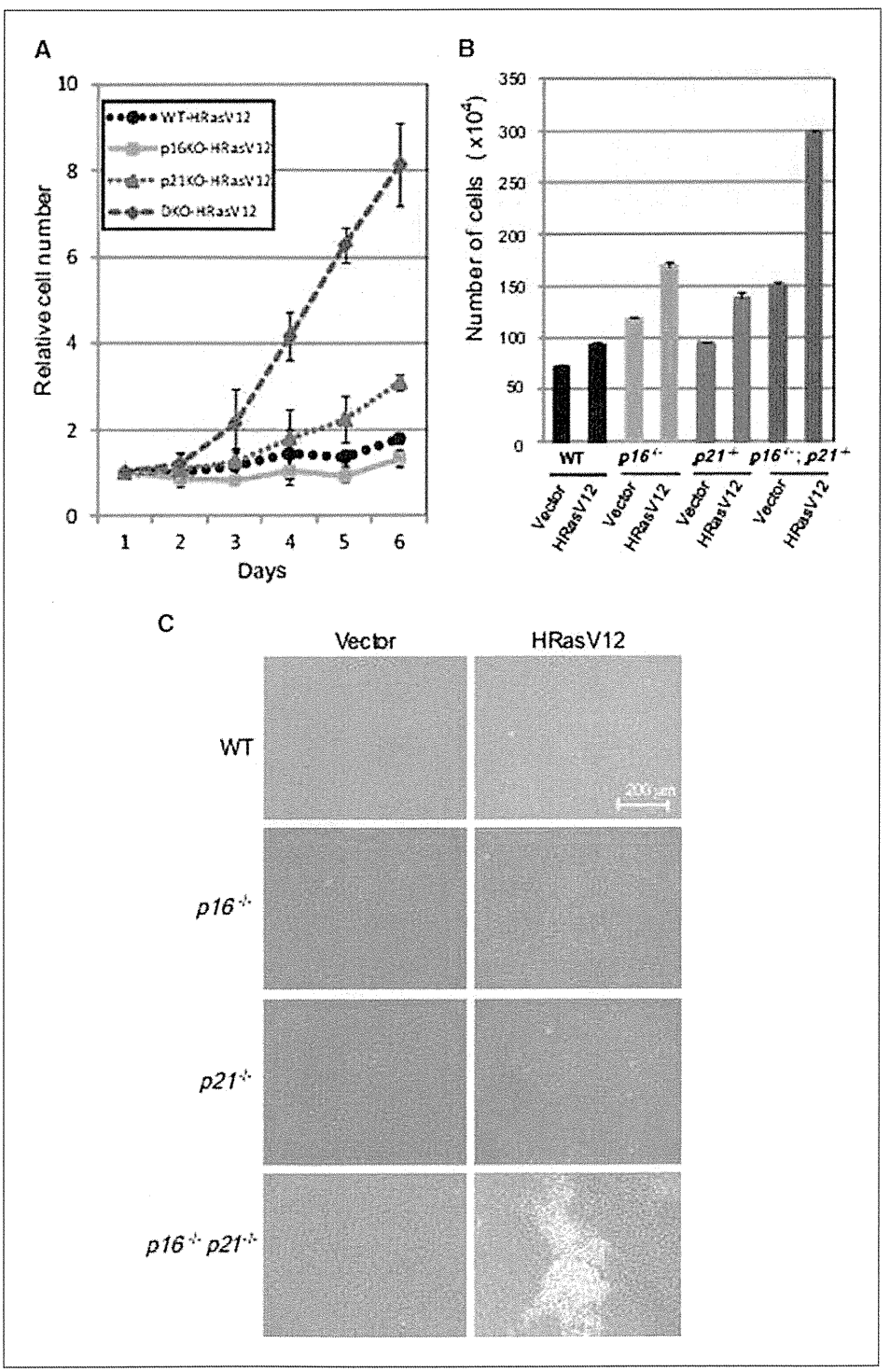

Figure 3. DKO MEFs escape contact inhibition. A, the cell numbers of wild-type, p16-KO, p21-KO, and DKO MEFs expressing oncogenic Ras were counted 7 d after retrovirus infection (indicated as day 1). The cells were counted in triplicate and the relative cell numbers are shown. B, relative cell numbers of wild-type, p16-KO, p21-KO, and DKO MEFs expressing oncogenic Ras in the focus formation assay. The means ± SD of triplicate experiments are shown. C, Ras-expressing immortalized DKO MEFs, but not the MEFs of other genotypes, formed foci after 15 d of culture. Representative data of three independent experiments are shown.

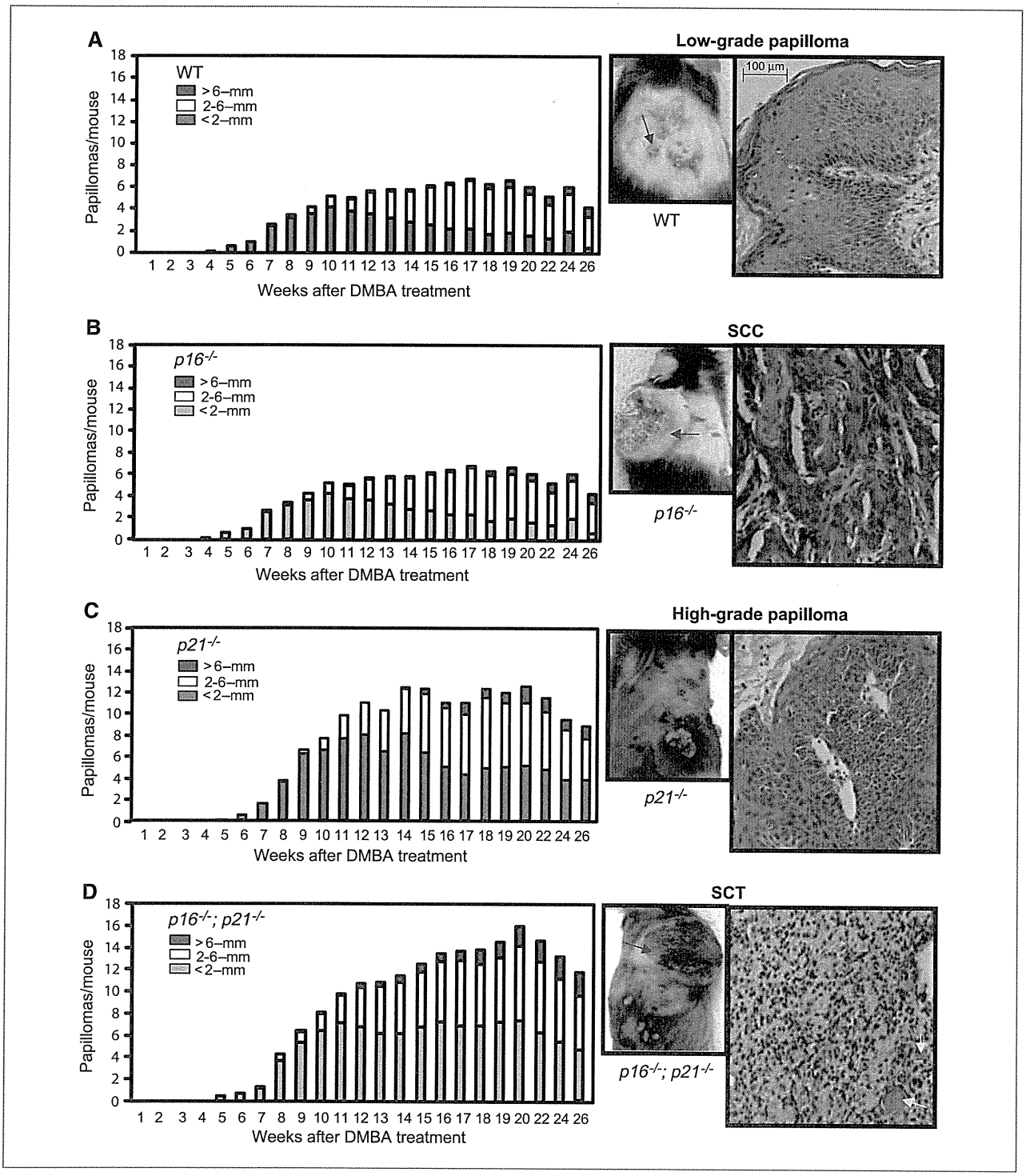

Figure 4. Analysis of DMBA/TPA–induced skin tumors. A to D, wild-type (n = 18; A), p16-KO (n = 13; B), p21-KO (n = 13; C), and DKO (n = 19; D) mice. Left, average number of papillomas at the indicated times and their relative size distribution. Middle, representative images of skin tumors at 30 wk after DMBA treatment. Right, histology of the representative tumors (indicated by red arrows in the tumor images; H&E staining; magnification, ×100). A, a low-grade papilloma showing thickening of epidermis with slight cellular atypia mainly in the parabasal layer and with hyperkeratosis. B, a large tumor with ulceration in the center of the tumor. Histologically, the tumor is diagnosed as squamous cell carcinoma (SCC) showing papillary proliferation of atypical epidermal cells with dyskeratosis. C, a high-grade papilloma showing papillary proliferation of the epidermis with cellular atypia, including high nucleus/cytoplasm (N/C) ratio, increase of nuclear chromatin, and increase of mitotic figures, although the polarity of maturation is still preserved. D, a spindle cell tumor (SCT), not otherwise specified, which showed diffuse proliferation of relatively uniform short spindle cells. Yellow arrows, muscle layers. Representative results of two independent experiments are shown.

conversion rate of benign papillomas in DKO mice (5.92%) was not increased compared with that in p16-KO mice (4.55%; Table 1). These results indicate that the high incidence of cancer in the mice with the DKO genotype is likely to be due to a cooperative effect of increased benign skin papilloma formation due to *p21$^{Waf1/Cip1}$* loss and increased malignant conversion of benign skin tumors due to *p16^{INK4a}* loss. It is also worth emphasizing that 31.6% (6 of 19) of the DKO mice developed malignant spindle cell tumors, which were more aggressively invasive through the muscle layers compared with squamous cell carcinomas (Fig. 4D; Table 1).

An intact DNA damage response prevents the progression of DMBA/TPA–induced skin tumors

It was reported that oncogenic Ras induces DNA damage signaling and the activation of the cell cycle checkpoint, which are critical for the cellular senescence and tumor suppression phenotypes (40–42). Therefore, we have examined γ-H2AX foci formation, a DNA damage response marker, in tumors in all the genotypes. γ-H2AX foci were detectable in a significant percentage of cells in the low-grade papillomas in the wild-type, p21-KO, and p16-KO mice. In contrast, a very small percentage of cells were positive for γ-H2AX foci in the low-grade papillomas that developed in DKO mice (Supplementary Fig. S4). These results suggest that p21$^{Waf1/Cip1}$ and p16^{INK4a} play important roles in conducting the DNA damage signaling pathway. Note that γ-H2AX foci were hardly detectable in most of the high-grade papillomas and malignant tumors, such as squamous cell carcinomas and spindle cell tumors, regardless of the genotype, suggesting that the higher-grade papillomas and the malignant tumors seem to have a defect in responding to DNA damage signals.

Discussion

In this study, we have generated for the first time the *p16^{INK4a};p21$^{Waf1/Cip1}$* double mutant mice (DKO mice) on a C57BL/6 background, a carcinogenesis-resistant strain, and analyzed the effects of *p16^{INK4a}* and *p21$^{Waf1/Cip1}$* deficiency on the susceptibility to cancer in cooperation with oncogenic Ras expression. MEFs derived from DKO mice easily escaped Ras-induced senescence and overrode contact inhibition in culture (Fig. 3). Moreover, DKO-mice on the C57BL/6 background were extremely susceptible to DMBA/TPA–induced skin carcinogenesis (Fig. 4). Our analyses clearly show a significant increase of cancer incidence in the DKO background because p21$^{Waf1/Cip1}$ deletion promotes benign skin tumor development and *p16^{INK4a}* deletion promotes the incidence of malignant conversion of benign skin tumors (Table 1).

There are reports showing that compound mice expressing a mutant form of CDK4 (CDK4-R24C), which is resistant to all of the p16^{INK4a} family members, on a *p21$^{Waf1/Cip1}$*-null background are more susceptible to malignant tumors compared with mice either lacking *p21$^{Waf1/Cip1}$* or expressing *CDK4-R24C* (27, 43). However, because CDK4-R24C has the ability to counteract all of the p16^{INK4a} family members, it has been unclear whether p16^{INK4a} or other p16^{INK4a} family members play a role in cooperating with p21$^{Waf1/Cip1}$ in the induction of cellular senescence and/or tumor suppression *in vivo*. Our study has clarified that the increased tumor incidence and immortalization of the previously described *cdk4r24c* mutant mice and MEFs with the *p21$^{Waf1/Cip1}$*-null background are most likely to be due to the absence of p16^{INK4a} from among the INK4 family both *in vitro* and *in vivo*.

It is also noteworthy that 31.6% of the DKO mice developed malignant spindle cell tumors, which were more aggressive

Table 1. Skin tumor susceptibility by DMBA/TPA in p16 and/or p21 knockout mice

	Mouse genotype			
	Wild-type (*n* = 18)	*p16$^{-/-}$* (*n* = 13)	*p21$^{-/-}$* (*n* = 13)	*p16$^{-/-}$;p21$^{-/-}$* (*n* = 19)
Tumor type, *n**				
Low-grade papilloma	16	5	4	2
High-grade papilloma	1	5	7	1
High-grade papilloma with microinvasion	0	0	2	1
Carcinoma *in situ*	1	1	0	1
Squamous cell carcinoma	0	2	0	8
Malignant spindle cell tumor	0	0	0	6
Mice with carcinomas, %	5.56	23.08	15.38	84.21
Maximum no. of papillomas/mouse	6.0	6.8	12.5	16.0
Malignant conversion ratio at 30 wk after DMBA (no. of carcinomas/total no. of papillomas), %	0.93	4.55†	1.23	5.92‡

NOTE: Tumors were analyzed 30 wk after DMBA treatment.
*The number of mice with the indicated tumors is shown.
†One *p16$^{-/-}$* mouse harbored two SCCs.
‡Two *p16$^{-/-}$;p21$^{-/-}$* mice harbored two SCCs.

than squamous cell carcinomas (Fig. 4D; Table 1). It is interesting that all of these spindle cell tumors exhibited a substantial increase in the expression of the *Oct4* gene, which is known to play an important role in stem cell maintenance and reprogramming (Supplementary Fig. S5), although the molecular mechanism behind this upregulation remains unclear. This is consistent in part with recent reports showing that both the $p16^{INK4a}$ and p53-$p21^{Waf1/Cip1}$ pathways play an inhibitory role in the reprogramming of differentiated cells toward becoming induced pluripotent stem cells (44–49). It is therefore tempting to speculate that the inactivation of both $p16^{Ink4a}$ and $p21^{Waf1/Cip1}$, in conjunction with Ras activation, increases the chance of reprogramming differentiated cells or stimulates the proliferation of undifferentiated cells *in vivo*. Further analysis is required to understand how the $p16^{Ink4a}$ and $p21^{Waf1/Cip1}$ pathways are linked to Oct4 expression.

It is still possible that the phenotypic effects seen in *$p16^{INK4a}$* knockout mice and DKO mice are compromised, at least to some extent, by developmental or somatic compensation by upregulation of the remaining $p16^{INK4a}$ family members (30–33). Nonetheless, our results provide direct evidence that $p16^{Ink4a}$ and $p21^{Waf1/Cip1}$ play cooperative roles in the onset and/or the maintenance of Ras-induced senescence *in vitro* and show for the first time that $p16^{INK4a}$ per se plays a crucial role in preventing the malignant conversion of benign skin tumors *in vivo*.

Disclosure of Potential Conflicts of Interest

No potential conflicts of interest were disclosed.

Acknowledgments

We thank Dr. P. Leder for *$p21^{Waf1/Cip1}$*-knockout mice, Dr. N.E. Sharpless for *$p16^{INK4a}$*-knockout mice, and Dr. M. Serrano [Spanish National Cancer Research Center (CNIO), Madrid, Spain] for retrovirus vector encoding H-RasV12. We also thank C. Sugita and S. Ohtomi for their assistance in mouse experiments.

Grant Support

Ministry of Education, Science, Sports and Technology of Japan, the Astellas Foundation for Research on Metabolic Disorders, the Vehicle Racing Commemorative Foundation, the Takeda Science Foundation, the Uehara Memorial Foundation, and the Mishima Kaiun Memorial Foundation.

The costs of publication of this article were defrayed in part by the payment of page charges. This article must therefore be hereby marked *advertisement* in accordance with 18 U.S.C. Section 1734 solely to indicate this fact.

Received 03/05/2010; revised 08/11/2010; accepted 09/15/2010; published OnlineFirst 11/09/2010.

References

1. Noda A, Ning Y, Venable SF, Pereira-Smith OM, Smith JR. Cloning of senescent cell-derived inhibitors of DNA synthesis using an expression screen. Exp Cell Res 1994;211:90–8.
2. Hara E, Smith R, Parry D, Tahara H, Stone S, Peters G. Regulation of $p16^{CDKN2}$ expression and its implications for cell immortalization and senescence. Mol Cell Biol 1996;16:859–67.
3. Alcorta DA, Xiong Y, Phelps D, Hannon G, Beach D, Barrett JC. Involvement of the cyclin-dependent kinase inhibitor $p16^{INK4a}$ in replicative senescence of normal human fibroblasts. Proc Natl Acad Sci U S A 1996;93:13742–7.
4. Serrano M, Lin AW, McCurrach ME, Beach D, Lowe SW. Oncogenic ras provokes premature cell senescence associated with accumulation of p53 and $p16^{INK4a}$. Cell 1997;88:593–602.
5. Randle DH, Zindy F, Sherr CJ, Roussel MF. Differential effects of $p19^{Arf}$ and $p16^{Ink4a}$ loss on senescence of murine bone marrow-derived preB cells and macrophages. Proc Natl Acad Sci U S A 2001;98:9654–9.
6. Takahashi A, Ohtani N, Yamakoshi K, et al. Mitogenic signalling and the $p16^{INK4a}$-Rb pathway cooperate to enforce irreversible cellular senescence. Nat Cell Biol 2006;8:1291–7.
7. McConnell BB, Gregory FJ, Stott FJ, Hara E, Peters G. Induced expression of $p16^{INK4a}$ inhibits both CDK4- and CDK2-associated kinase activity by reassortment of cyclin-CDK-inhibitor complexes. Mol Cell Biol 1999;19:1981–9.
8. Mitra J, Dai CY, Somasundaram K, et al. Induction of $p21^{WAF1/CIP1}$ and inhibition of Cdk2 mediated by the tumor suppressor $p16^{INK4a}$. Mol Cell Biol 1999;19:3916–28.
9. Sherr CJ, Roberts JM. CDK inhibitors: positive and negative regulators of G_1-phase progression. Genes Dev 1999;13:1501–12.
10. Li W, Kotoshiba S, Berthet C, Hilton MB, Kaldis P. Rb/Cdk2/Cdk4 triple mutant mice elicit an alternative mechanism for regulation of the G_1-S transition. Proc Natl Acad Sci U S A 2009;106:486–91.
11. Collado M, Blasco MA, Serrano M. Cellular senescence in cancer and aging. Cell 2007;130:223–33.
12. Jacobs JJ, de Lange T. $p16^{INK4a}$ as a second effector of the telomere damage pathway. Cell Cycle 2005;4:1364–8.
13. Ben-Porath I, Weinberg RA. When cells get stressed: an integrative view of cellular senescence. J Clin Invest 2004;113:8–13.
14. Okada H, Mak TW. Pathways of apoptotic and non-apoptotic death in tumor cells. Nat Rev Cancer 2004;4:592–603.
15. Sharpless NE, DePinho RA. Cancer: crime and punishment. Nature 2005;436:636–7.
16. Campisi J. Senescent cells, tumor suppression, and organismal aging: good citizens, bad neighbors. Cell 2005;F120:513–22.
17. Pei XH, Xiong Y. Biochemical and cellular mechanisms of mammalian CDK inhibitors: a few unresolved issues. Oncogene 2005; 24:2787–95.
18. Krimpenfort P, Quon KC, Mooi WJ, Loonstra A, Berns A. Loss of $p16^{INK4a}$ confers susceptibility to metastatic melanoma in mice. Nature 2001;413:83–6.
19. Sharpless NE, Bardeesy N, Lee KH, et al. Loss of $p16^{INK4a}$ with retention of $p19^{Arf}$ predisposes mice to tumorigenesis. Nature 2001; 413:86–91.
20. Deng C, Zhang P, Harper JW, Elledge SJ, Leder P. Mice lacking $p21^{Waf1/Cip1}$ undergo normal development, but are defective in G_1 checkpoint control. Cell 1995;82:675–84.
21. Brugarolas J, Chandrasekaran C, Gordon JI, Beach D, Jacks T, Hannon GJ. Radiation-induced cell cycle arrest compromised by p21 deficiency. Nature 1995;377:552–7.
22. Martín-Caballero J, Flores JM, García-Palencia P, Serrano M. Tumor susceptibility of $p21^{Waf1/Cip1}$-deficient mice. Cancer Res 2001;61: 6234–8.
23. DiGiovanni J, Prichett WP, Decina PC, Diamond L. DBA/2 mice are as sensitive as SENCAR mice to skin tumor promotion by 12-O-tetradecanoylphorbol-13-acetate. Carcinogenesis 1984;5:1493–8.
24. Hennings H, Glick AB, Lowry DT, Krsmanovic LS, Sly LM, Yuspa SH. FVB/N mice: an inbred strain sensitive to the chemical induction of squamous cell carcinomas in the skin. Carcinogenesis 1993;14: 2353–8.
25. Woodworth CD, Michael E, Smith L, et al. Strain-dependent differences in malignant conversion of mouse skin tumors is an inherent property of the epidermal keratinocyte. Carcinogenesis 2004;25: 1771–8.
26. Pantoja C, Serrano M. Murine fibroblasts lacking p21 undergo senescence and are resistant to transformation by oncogenic Ras. Oncogene 1999;18:4974–82.

27. Carbone CJ, Grana X, Reddy EP, Haines DS. p21 loss cooperates with INK4 inactivation facilitating immortalization and bcl-2-mediated anchorage-independent growth of oncogene-transduced primary mouse fibroblasts. Cancer Res 2007;67:4130–7.
28. Dimri GP, Lee X, Basile G, et al. A biomarker that identifies senescent human cells in culture and in aging skin *in vivo*. Proc Natl Acad Sci U S A 1995;92:9363–7.
29. Yamakoshi K, Takahashi A, Hirota F, et al. Real-time *in vivo* imaging of $p16^{Ink4a}$ reveals cross talk with p53. J Cell Biol 2009;186:393–407.
30. Krimpenfort P, Ijpenberg A, Song JY, et al. $p15^{INK4b}$ is a critical tumor suppressor in the absences of $p16^{INK4a}$. Nature 2007;448:943–6.
31. Ramsey MR, Krishnamurthy J, Pei XH, et al. Expression of $p16^{Ink4a}$ compensates for $p18^{Ink4c}$ loss in cyclin-dependent kinase 4/6-dependent tumors and tissues. Cancer Res 2007;67:4732–41.
32. Wiedemeyer R, Brennan C, Heffernan TP, et al. Feedback circuit among INK4 tumor suppressors constrains human glioblastoma development. Cancer Cell 2008;13:355–64.
33. Ciemerych MA, Sicinski P. Cell cycle in mouse development. Oncogene 2005;24:2877–98.
34. Parrinello S, Samper E, Krtolica A, Goldstein J, Melov S, Campisi J. Oxygen sensitivity severely limits the replicative lifespan of murine fibroblasts. Nat Cell Biol 2003;5:741–7.
35. Kamijo T, Zindy F, Roussel MF, et al. Tumor suppression at the mouse INK4a locus mediated by the alternative reading frame product $p19^{ARF}$. Cell 1997;91:649–59.
36. Stott FJ, Bates S, James MC, et al. The alternative product from the human CDKN2A locus, $p14^{ARF}$, participates in a regulatory feedback loop with p53 and MDM2. EMBO J 1998;17:5001–14.
37. Kemp CJ. Multistep skin cancer in mice as a model to study the evolution of cancer cells. Semin Cancer Biol 2005;15:460–73.
38. Weinberg WC, Fernandez-Salas E, Morgan DL, et al. Genetic deletion of $p21^{WAF}1$ enhances papilloma formation but not malignant conversion in experimental mouse skin carcinogenesis. Cancer Res 1999;59:2050–4.
39. Topley GI, Okuyama R, Gonzales JG, Conti C, Dotto GP. $p21^{WAF1/Cip1}$ functions as a suppressor of malignant skin tumor formation and a determinant of keratinocyte stem-cell potential. Proc Natl Acad Sci U S A 1999;96:9089–94.
40. Di Micco R, Fumagalli M, Cicalese A, et al. Oncogene-induced senescence is a DNA damage response triggered by DNA hyper-replication v. Nature 2006;444:638–42.
41. Bartkova J, Rezaei N, Liontos M, et al. Oncogene-induced senescence is part of the tumorigenesis barrier imposed by DNA damage checkpoints. Nature 2006;444:633–7.
42. Halazonetis TD, Gorgoulis VG, Bartek J. An oncogene-induced DNA damage model for cancer development. Science 2008;319:1352–5.
43. Quereda V, Martinalbo J, Dubus P, Carnero A, Malumbres M. Genetic cooperation between $p21^{Cip1}$ and INK4 inhibitors in cellular senescence and tumor suppression. Oncogene 2007;26:7665–74.
44. Hong H, Takahashi K, Ichisaka T, et al. Suppression of induced pluripotent stem cell generation by the p53–21 pathway. Nature 2009;460:1132–5.
45. Utikal J, Polo JM, Stadtfeld M, et al. Immortalization eliminates a roadblock during cellular reprogramming into iPS cells. Nature 2009;460:1145–8.
46. Marión RM, Strati K, Li H, et al. A p53-mediated DNA damage response limits reprogramming to ensure iPS cell genomic integrity. Nature 2009;460:1149–53.
47. Li H, Collado M, Villasante A, et al. The Ink4/Arf locus is a barrier for iPS cell reprogramming. Nature 2009;460:1136–9.
48. Kawamura T, Suzuki J, Wang YV, et al. Linking the p53 tumour suppressor pathway to somatic cell reprogramming. Nature 2009;460:1140–4.
49. Banito A, Rashid ST, Acosta JC, et al. Senescence impairs successful reprogramming to pluripotent stem cells. Genes Dev 2009;23:2134–9.

original article

Annals of Oncology 20: 526–533, 2009
doi:10.1093/annonc/mdn677
Published online 12 December 2008

Soluble interleukin-2 receptor retains prognostic value in patients with diffuse large B-cell lymphoma receiving rituximab plus CHOP (RCHOP) therapy

D. Ennishi[1,5], M. Yokoyama[1], Y. Terui[1], H. Asai[1], S. Sakajiri[1], Y. Mishima[1], S. Takahashi[1], H. Komatsu[2], K. Ikeda[3], K. Takeuchi[4], M. Tanimoto[5] & K. Hatake[1]*

[1]*Department of Medical Oncology and Hematology, Cancer Institute Hospital, Tokyo;* [2]*Department of Epidemiology;* [3]*Department of Transfusion Medicine, Okayama University Graduate School of Medicine, Dentistry and Pharmaceutical Sciences, Okayama;* [4]*Devision of Pathology, The Japanese Foundation for Cancer Research, Tokyo;* [5]*Department of Hematology and Oncology, Okayama University Graduate School of Medicine, Dentistry and Pharmaceutical Sciences, Okayama, Japan*

Received 5 July 2008; revised 11 September 2008; accepted 16 September 2008

Background: Soluble interleukin-2 receptor (SIL-2R) is known to be a prognostic parameter in patients with diffuse large B-cell lymphoma (DLBCL) receiving cyclophosphamide, doxorubicin, vincristine and prednisone (CHOP) therapy. However, its prognostic value has not been well known since the introduction of rituximab.

Patients and methods: We retrospectively evaluated the prognostic impact of SIL-2R in 228 DLBCL patients, comparing 141 rituximab-combined CHOP (RCHOP)-treated patients with 87 CHOP-treated patients as a historical control.

Results: Patients with high serum SIL-2R showed significantly poorer event-free survival (EFS) and overall survival (OS) than patients with low SIL-2R in both the RCHOP group (2-year EFS, 66% versus 92%, $P < 0.001$; OS, 82% versus 95%, $P = 0.005$) and the CHOP group (2-year EFS, 40% versus 82%; OS, 61% versus 90%, both $P < 0.001$). Multivariate analysis including the five parameters of International Prognostic Index (IPI) and two-categorized IPI revealed that SIL-2R was an independent prognostic factor for EFS and OS in the RCHOP group as well as in the CHOP group.

Conclusions: Our results demonstrate that SIL-2R retains its prognostic value in the rituximab era. The prognostic value of SIL-2R in DLBCL patients receiving rituximab-combined chemotherapy should be reassessed on a larger scale and by long-term follow-up.

Key words: diffuse large B-cell lymphoma, rituximab, soluble interleukin-2 receptor

introduction

Diffuse large B-cell lymphoma (DLBCL) is the most common subtype of non-Hodgkin's lymphoma [1]. It takes an aggressive clinical course and comprises a heterogeneous group of lymphomas in terms of morphology, phenotype, molecular biology and clinical behavior. Up to now, the International Prognostic Index (IPI) has been the most widely used predictive model for patients with DLBCL treated with cyclophosphamide, doxorubicin, vincristine and prednisone (CHOP) [2]. On the other hand, soluble interleukin-2 receptor (SIL-2R) has also been investigated as a prognostic factor, and several studies have demonstrated that a high level of SIL-2R before treatment is associated with both a low remission rate and poor prognosis [3–8].

SIL-2R is the soluble form of interleukin-2 receptor (IL-2R). IL-2R is expressed on the cell membrane of lymphocytes and plays important roles in their activation and proliferation [9]. It is composed of at least three glycoprotein chains: α (55 kDa), β (75 kDa) and γ (64 kDa). Each subunit is able to bind to the ligand independently with either low (IL-2Rα) or intermediate (IL-2Rβ and γ) affinity. It is now possible to examine the expression of the soluble-type α subunit [10]. The soluble IL-2Rα chain is induced and expressed only after mononuclear cell (T cell, B cell, monocyte, and natural killer cell) activation [11, 12]. Therefore, activated T and B cells have elevated levels of SIL-2R.

Although the CHOP regimen has been the mainstay of treatment for aggressive lymphomas for several decades [13], treatment outcome has significantly improved with the introduction of rituximab (an anti-CD20 chimeric antibody) in both young and elderly patients [14–17]. Since the introduction of rituximab, several prognostic factors have been reevaluated. Sehn et al. [18] recently reevaluated five prognostic

Correspondence to: Dr Kiyohiko Hatake, Department of Medical Oncology and Hematology, Cancer Institute Hospital, 3-10-6 Ariake Koto-ku, Tokyo 135-8550, Japan. Tel: +81-3-3520-0111; Fax: +81-3-3570-0343; E-mail: khatake@jfcr.or.jp

factors and demonstrated that the IPI remained predictive; they proposed a revised IPI in which DLBCL patients are classified into very good (no IPI risk factors), good (one to two risk factors) and poor (three to five risk factors) categories. In contrast, BCL2, BCL6 and immunohistochemically defined germinal center (GC) phenotype have been reported to have no prognostic value when rituximab is added to chemotherapy [19–24]. Other clinical factors or biomarkers identified in patients receiving CHOP therefore need to be reassessed in patients treated with CHOP combined with rituximab.

Up to now, the prognostic value of SIL-2R in RCHOP has not been investigated. The aim of the present study was to retrospectively reassess the prognostic value of SIL-2R in DLBCL patients receiving RCHOP as compared with CHOP alone and to investigate whether or not this factor still influences the outcome of DLBCL.

patients and methods

patient characteristics

In the present study, we reviewed the medical records of patients with CD20-positive DLBCL who received CHOP with or without rituximab as a first-line therapy at the Cancer Institute Hospital from January 2000 to December 2006 and were followed until January 2008. The study protocol and sampling were approved by the Institutional Review Board of the Cancer Institute Hospital. Informed consent for retrospective analysis and additional immunophenotypic analysis and gene rearrangement studies was obtained.

Patients were analyzed if they were older than 18 years and had a performance status (PS) of zero to three according to the criteria of the European Cooperative Oncology Group. Patients were excluded if they had clinically relevant cardiac diseases or positivity for antibodies against HIV-1 or 2. Patients with primary mediastinal large B-cell lymphoma, primary CNS lymphoma and primary testicular lymphoma were also not included in this study.

The disease stage was evaluated according to the Ann Arbor staging system. All patients had undergone staging investigations, including physical examinations, blood and serum analysis, bone marrow aspiration and biopsy and computed tomography of the neck, chest, abdomen and pelvis. Magnetic resonance imaging was used for evaluation of involved organs in the head and neck. The following clinical and laboratory data were available at the time of diagnosis: age, sex, serum lactate dehydrogenase level, PS, presence of B symptoms, clinical stage and number of extranodal sites. This allowed the IPI scores to be determined in the studied patients. Patients were categorized into either a low-risk group (IPI score, 0–2) or a high-risk group (IPI score, 3–5). Response to initial therapy was evaluated according to the Cheson criteria [25].

treatment

In both the CHOP and RCHOP groups, CHOP chemotherapy was given triweekly at a standard dose. Patients with stages IB–IV received six cycles, and patients with stage IA three cycles, of CHOP chemotherapy followed by radiotherapy for the involved field. After incorporation of rituximab into the CHOP regimen in February 2004, patients were treated with RCHOP regimen, in which rituximab was administered at a standard dose of 375 mg/m^2 once weekly for 8 weeks concurrently with triweekly CHOP, as described previously [26].

chemical studies

The serum SIL-2R levels were determined using a sandwich enzyme-linked immunosorbent assay kit (Cell-free Interleukin-2 Receptor Test Kit, T Cell Science, Cambridge, MA) using two mAbs against distinct two different epitopes of the p55 alpha-chain of the IL-2R complex. Serum SIL-2R was considered 'high' when higher than the median and 'low' when lower than the median.

pathological studies

Biopsy samples collected before treatment were fixed in formalin, embedded in paraffin, sliced and stained with hematoxylin and eosin for morphological analysis. For diagnosis of DLBCL, immunohistochemical analysis was carried out using the dextran-polymer method (EnVision+; Dako, Glostrup, Denmark) with mAbs against CD5, CD10, CD20, Ki67, BCL2, BCL6 and MUM1 in most cases and with CyclinD1 to exclude the possibility of a pleomorphic variant of mantle cell lymphoma when the lymphoma was CD5 positive. Patients with a small-cell component implying transformation from low-grade/indolent B-cell lymphoma were excluded. All the samples were reviewed by an expert hematopathologist (KT).

statistical analysis

Basic characteristics of the CHOP group and RCHOP group were compared by Fisher's exact test. Event-free survival (EFS) was calculated from the date of diagnosis to the date of documented disease progression, relapse or death from any cause or to the stopping date. Overall survival (OS) was calculated from the date of diagnosis until death from any cause or the last follow-up. If the stopping date was not reached, the data were censored at the date of the last follow-up evaluation. Survival curves were estimated by the Kaplan–Meier method, and overall differences were compared by the log-rank test. Log-rank test was carried out according to SIL-2R, two-categorized IPI for the two treatment groups. To estimate the unbiased prognostic impacts of SIL-2R on EFS and OS, Cox proportional hazards analysis was applied. First, we conducted univariate Cox analysis for SIL-2L, all IPI factors and dichotomized IPI and then we carried out multivariate Cox analysis adjusted for SIL-2R and each of the IPI risk factors, with final adjustment for SIL-2R and dichotomized IPI. Only factors that were associated with at least a trend toward significance in the univariate analysis (unadjusted P value <0.20) were evaluated in the multivariate model. We set $P < 0.05$ as the level of statistical significance. Data were analyzed using SPSS software version 11.0 for Windows (SPSS, Chicago, IL).

results

patient characteristics

A total of 228 patients were analyzed, of whom 87 (38.2%) were given CHOP and 141 (61.8%) were given RCHOP. The median SIL-2R was 1005.5 mg/dl (range 220–35 600), and high SIL-2R was observed in 114 (50.0%) patients: 40 of 87 (46.0%) in the CHOP group and 74 of 141 (52.5%) in the RCHOP group. There was no significant difference in the proportion of high SIL-2R patients between the two treatment groups. The characteristics of the patients are listed in Table 1. Patient and disease characteristics were well balanced between the groups.

survival analysis

With median follow-up periods of 30 months in the RCHOP group and 44 months in the CHOP group, EFS rates at 2 years were 78% and 65%, respectively ($P = 0.030$), and OS rates at 2 years were 89% and 81%, respectively ($P = 0.040$).

Table 1. Patients' characteristics according to serum SIL-2R level for CHOP and RCHOP group

Characteristics	CHOP group			RCHOP group			*P*, all
	All	Low SIL2R	High SIL2R	All	Low SIL2R	High SIL2R	
No. of patients (%)	87(100)	47 (54)	40 (46)	141 (100)	67 (48)	74 (52)	
Sex, no. (%)							0.41
Male	50 (57)	27 (57)	23 (58)	72 (51)	27 (40)	45 (61)	
Female	37 (43)	20 (43)	17 (42)	69 (49)	40 (60)	29 (39)	
Age, no. (%)							0.52
≤60	24 (28)	13 (28)	11 (28)	45 (32)	29 (43)	16 (22)	
>60	63 (72)	34 (72)	29 (72)	96 (68)	38 (57)	58 (78)	
LDH, no. (%)							0.54
Normal	29 (32)	22 (35)	7 (17)	68 (48)	45 (67)	23 (31)	
High	58 (68)	25 (65)	33 (83)	73 (52)	22 (33)	51 (69)	
PS, no. (%)							0.81
0–1	77 (89)	44 (94)	33 (83)	127 (90)	66 (98)	61 (82)	
2–3	10 (11)	3 (6)	7 (17)	14 (10)	1 (2)	13 (18)	
Stage, no. (%)							0.73
I, II	55 (63)	40 (85)	15 (38)	93 (66)	57 (85)	36 (49)	
III, IV	32 (37)	7 (15)	25 (72)	48 (34)	10 (15)	38 (51)	
Extranodal sites, no. (%)							0.84
0, 1	67 (77)	43 (91)	24 (60)	106 (75)	63 (94)	43 (57)	
≤2	20 (23)	4 (9)	16 (40)	35 (25)	4 (6)	31 (43)	
IPI, no. (%)							0.86
L/L-I	60 (69)	40 (85)	20 (50)	100 (71)	63 (94)	37 (50)	
H/H-I	27 (31)	7 (15)	20 (50)	41 (29)	4 (6)	37 (50)	

SIL2R, soluble interleukin-2 receptor; CHOP, cyclophosphamide, doxorubicin, vincristine and prednisone; RCHOP, rituximab-combined CHOP; LDH, lactate dehydrogenase; PS, performance status; IPI, International Prognostic Index; L/L-I, low or low-intermediate; H/H-I, high or high-intermediate; high SIL-2R; SIL-2R >1000 U/ml, low SIL-2R; SIL-2R ≤1000 U/ml.

For CHOP therapy, the EFS and OS rates at 2 years were 82% and 93% for low SIL-2R and 43% and 65% for high SIL-2R, respectively. The differences in both the EFS and OS rates between the two SIL-2R levels were significant (both $P < 0.001$) (Figure 1A and B). In the RCHOP group, the EFS and OS rates at 2 years were 90% and 95% for low SIL-2R and 66% and 84% for high SIL-2R, respectively. The differences in both EFS and OS rates between the two SIL-2R levels were significant (EFS, $P < 0.001$; OS $P = 0.005$) (Figure 1C and D).

To study the impact of rituximab on the predictive value, we examined the clinical outcome according to treatment in the SIL-2R low and high groups. The patients with high SIL-2R who received RCHOP therapy had a significantly better OS at 2 years than patients treated with CHOP alone (84% versus 65%, $P = 0.020$). The EFS at 2 years was estimated to be 66% for the RCHOP group and 43% for the CHOP group ($P = 0.010$). For the patients with low SIL-2R, the influence of rituximab on OS and EFS was not significant (OS, 93% versus 95%, $P = 0.310$; EFS, 82% versus 90%, $P = 0.160$) (Table 2).

For comparison with this parameter, we analyzed the survival curves according to the IPI in both treatment groups. The EFS and OS rates at 2 years were 35% and 59% for high or high-intermediate IPI and 77% and 91% for low or low-intermediate IPI, respectively, in the CHOP group. The differences in both EFS and OS rates between the two IPI groups were significant (both $P < 0.001$). Similarly, the EFS and OS rates were 58% and 80% for high or high-intermediate IPI and 86% and 94% for low or low-intermediate IPI, respectively, in the RCHOP group. Again, the differences in the EFS and OS rates were significant ($P < 0.001$ and $P = 0.004$, respectively).

To estimate unbiased prognostic impacts, Cox univariate analysis showed that a high SIL-2R level, high PS, advanced stage, multiple extranodal sites and high or high-intermediate risk of IPI were associated with poor EFS and OS in both treatment groups (Table 3). In the second step, Cox multivariate analysis showed that only SIL-2R was significantly associated with a higher risk of event and that SIL-2R and PS were independently associated with poor OS in both treatment groups (Table 4). Finally, SIL-2R was a significant risk factor for EFS and a borderline risk factor for OS in both the CHOP and RCHOP groups ($P = 0.060$ and 0.070, respectively), whereas IPI was a significant risk factor for EFS and OS in the CHOP group and a borderline significant risk factor for EFS and OS ($P = 0.070$ and 0.080, respectively) in the RCHOP group (Table 5).

discussion

Although SIL-2R is easy to measure, its prognostic value has been underestimated due to its evaluation in smaller populations than those for other parameters, such as IPI [2]. The SIL-2R level was reported to be significantly high in highly aggressive lymphomas [6] and subsequently was recognized to reflect tumor burden and poor outcome [3–8]. However, these

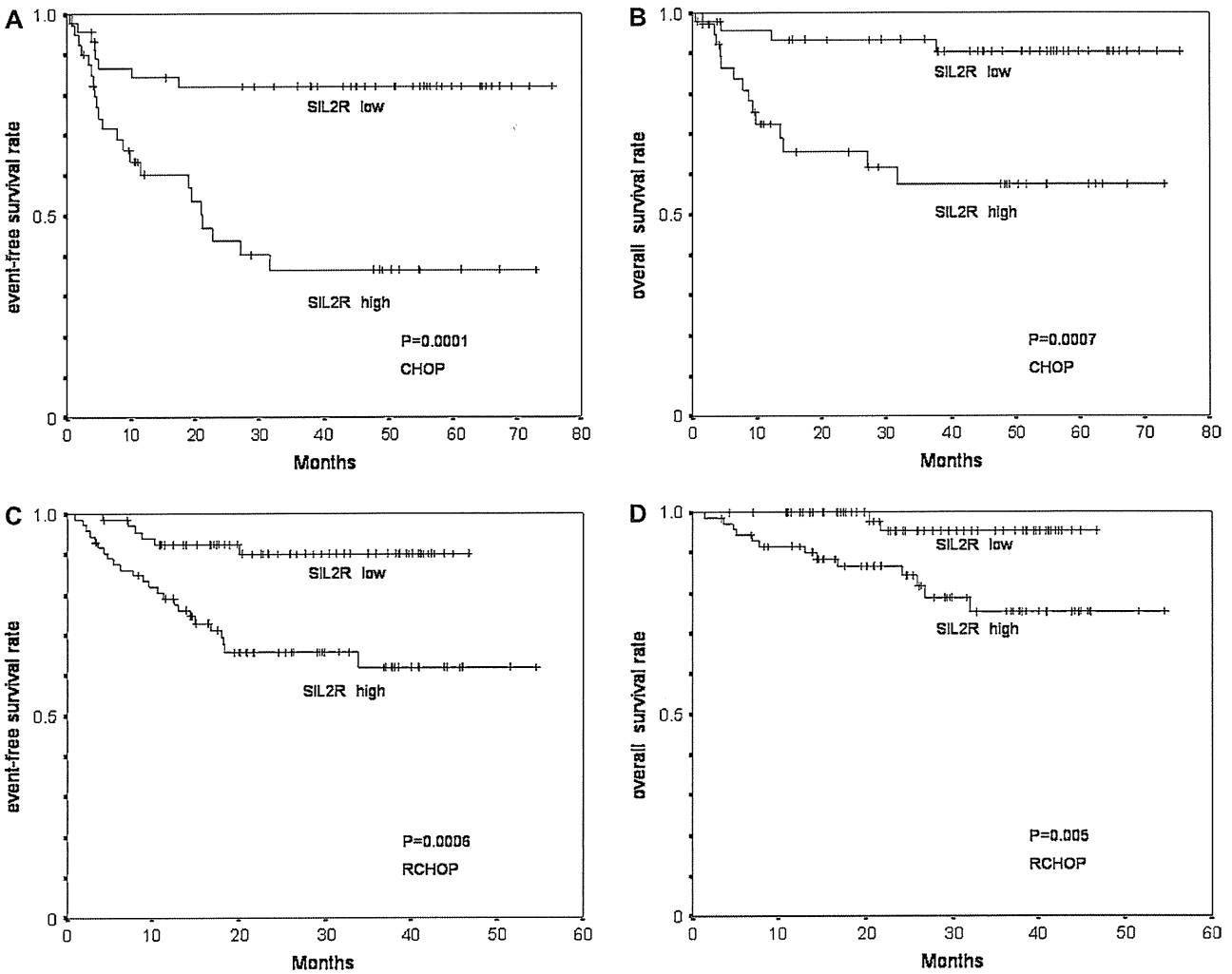

Figure 1. Event-free survival (EFS) and overall survival (OS) curves for diffuse large B-cell lymphoma patients treated with cyclophosphamide, doxorubicin, vincristine and prednisone (CHOP) and rituximab-combined CHOP (RCHOP) in relation to soluble interleukin-2 receptor (SIL-2R). EFS (A) and OS (B) curves according to low ($n = 47$) versus high ($n = 40$) SIL-2R in the CHOP group. EFS (C) and OS (D) curves according to low ($n = 67$) versus high ($n = 74$) SIL-2R in the RCHOP group.

Table 2. Analysis of 2-year survival rate according to CHOP and RCHOP therapy in both SIL-2R groups

Clinical outcome	Low SIL-2R			High SIL-2R		
	CHOP	RCHOP	*P*	CHOP	RCHOP	*P*
2-year survival						
EFS (%)	82	90	0.160	43	66	0.0010
OS (%)	93	95	0.310	65	84	0.0020

CHOP, cyclophosphamide, doxorubicin, vincristine and prednisone; RCHOP, rituximab-combined CHOP; SIL2R, soluble interleukin-2 receptor; EFS, event-free survival; OS, overall survival.

results were obtained in patients receiving chemotherapy, and the prognostic value of SIL-2R has not been assessed in rituximab-combined treatment.

In the present study, univariate analysis showed that SIL-2R retained its prognostic value in DLBCL patients treated with RCHOP, as well as in those receiving CHOP alone. Multivariate analysis also showed that SIL-2R was an independent significant prognostic factor after adjustment for IPI risk factors and independently associated with significantly decreased EFS and moderately decreased OS after adjustment by two-categorized IPI in both the CHOP and RCHOP groups. On the other hand, the clinical outcome of patients with high SIL-2R was significantly improved by addition of rituximab to the chemotherapy, in contrast to the lack of any difference in the patients with low SIL-2R. To our knowledge, this is the first report to demonstrate the prognostic value of SIL-2R in DLBCL patients treated with rituximab-combined chemotherapy.

Although the present study was not a randomized prospective one, and possibly biased by factors other than IPI and SIL-2R, the distribution of baseline characteristics, including IPI factors, was similar between the two treatment groups. On the other hand, the population employed in the present analysis had more limited disease and a favorable IPI score compared with those in previous studies of DLBCL [13–17]. This might account for the better outcome of our

Table 3. The effects of clinical factors on EFS and OS in CHOP by univariate analysis using Cox proportional hazard model

	Variable	HR	95% CI	*P* value
CHOP				
EFS	SIL-2R			
	Low	1.00		
	High	4.30	1.94–9.74	<0.001
	Age			
	≤60	1.00		
	>60	1.48	0.64–3.46	0.36
	LDH			
	Normal	1.00		
	High	2.65	0.80–8.74	0.11
	PS			
	0–1	1.00		
	2–3	4.10	1.64–10.25	0.003
	Stage			
	I, II	1.00		
	III, IV	3.75	1.79–7.83	<0.001
	Extranodal sites			
	0–1	1.00		
	≤2	3.24	1.54–6.81	0.002
	IPI			
	L/L-I	1.00		
	H/H-I	3.97	1.91–8.25	<0.001
OS	SIL-2R			
	Low	1.00		
	High	5.64	1.84–17.23	0.002
	Age			
	≤60	1.00		
	>60	2.20	0.64–7.61	0.21
	LDH			
	Normal	1.00		
	High	4.71	0.63–35.41	0.13
	PS			
	0–1	1.00		
	2–3	7.18	2.44–21.13	<0.001
	Stage			
	I, II	1.00		
	III, IV	5.15	1.92–13.81	0.001
	Extranodal sites			
	0-1	1.00		
	≤2	4.24	1.64–10.98	0.003
	IPI			
	L/L-I	1.00		
	H/H-I	7.28	2.69–19.67	<0.001
RCHOP				
EFS	SIL-2R			
	Low	1.00		
	High	4.20	1.72–10.33	0.002
	Age			
	≤60	1.00		
	>60	1.38	0.61–3.11	0.44
	LDH			
	Normal	1.00		
	High	1.41	0.68–2.93	0.35
	PS			
	0–1	1.00		
	2–3	3.62	1.35–8.46	0.003
	Stage			
	I, II	1.00		
	III, IV	3.42	1.64–7.11	0.001
	Extranodal sites			
	0–1	1.00		
	≤2	3.43	1.67–7.03	<0.001
	IPI			
	L/L-I	1.00		
	H/H-I	3.40	1.82–6.25	<0.001
OS	SIL-2R			
	Low	1.00		
	High	6.42	1.45–28.45	0.01
	Age			
	≤60	1.00		
	>60	3.50	0.79–15.52	0.10
	LDH			
	Normal	1.00		
	High	1.69	0.58–4.97	0.34
	PS			
	0–1	1.00		
	2–3	5.97	2.03–17.54	0.001
	Stage			
	I, II	1.00		
	III, IV	2.46	0.89–6.79	0.08
	Extranodal sites			
	0–1	1.00		
	≤2	2.65	0.96–7.33	0.06
	IPI			
	L/L-I	1.00		
	H/H-I	4.03	1.43–11.34	0.08

EFS, event-free survival; OS, overall survival; CHOP, cyclophosphamide, doxorubicin, vincristine and prednisone; RCHOP, rituximab-combined CHOP; HR, hazard ratio; CI, confidential interval; SIL2R, soluble interleukin-2 receptor; LDH, lactate dehydrogenase; PS, performance status; IPI, International Prognostic Index; L/L-I, low or low-intermediate; H/H-I, high or high-intermediate.

patients than for those in previous reports such as that by Coiffier et al. [14] who observed 2-year survival rates of 70% and 57% in elderly patients treated with RCHOP and CHOP, respectively. Even with the excellent outcome we observed, however, the prognostic value of SIL-2R was significant and greater than that of other IPI risk factors. To allow our present results to be generalized to routine patient care, these findings should be validated in a variety of patient populations.

A number of prognostic markers have been identified in patients with DLBCL treated by chemotherapy alone [19–21], some of which have been reassessed and shown not to be associated with prognosis in patients receiving rituximab-combined chemotherapy [22–24]. BCL2 overexpression was reported to be associated with poorer survival in patients treated with CHOP-like regimens [19], but its prognostic value was not confirmed in patients receiving rituximab-combined chemotherapy in several studies, indicating that addition of rituximab overcomes the negative influence of BCL2

Table 4. Multivariate Cox proportional hazard regression analysis for SIL-2R and IPI risk factors in both treatment groups

	Variable	HR	95% CI	*P* value
CHOP				
EFS	SIL-2R			
	Low	1.00		
	High	2.74	1.05–7.14	0.04
	PS			
	0–1	1.00		
	2–3	2.12	0.73–6.14	0.17
	Stage			
	I, II	1.00		
	III, IV	1.82	0.65–5.09	0.25
	Extranodal sites			
	0–1	1.00		
	≤2	1.09	0.38–3.10	0.87
OS	SIL-2R			
	Low	1.00		
	High	3.53	1.03–12.95	0.05
	LDH			
	Normal	1.00		
	High	3.21	0.40–25.51	0.27
	PS			
	0–1	1.00		
	2–3	3.60	0.98–13.20	0.05
	Stage			
	I, II	1.00		
	III, IV	2.00	0.51–7.87	0.32
	Extranodal sites			
	0–1	1.00		
	≤2	0.86	0.22-0.83	0.83
RCHOP				
EFS	SIL-2R			
	Low	1.00		
	High	2.65	1.01–7.30	0.05
	PS			
	0–1	1.00		
	2–3	1.66	0.62–4.42	0.31
	Stage			
	I, II	1.00		
	III, IV	1.69	0.65–4.42	0.28
	Extranodal sites			
	0–1	1.00		
	≤2	1.36	0.50–3.67	0.55
OS	SIL-2R			
	Low	1.00		
	High	5.09	1.00–25.88	0.05
	Age			
	≤60	1.00		
	>60	2.45	0.54–11.17	0.24
	PS			
	0–1	1.00		
	2–3	4.49	1.15–17.45	0.03
	Stage			
	I, II	1.00		
	III, IV	1.02	0.23–4.45	0.98
	Extranodal sites			
	0–1	1.00		
	≤2	0.70	0.15–3.39	0.66

SIL2R, soluble interleukin-2 receptor; IPI, International Prognostic Index; CHOP, cyclophosphamide, doxorubicin, vincristine and prednisone; HR, hazard ratio; CI, confidential interval; EFS, event-free survival; PS, performance status; OS, overall survival; LDH, lactate dehydrogenase; RCHOP, rituximab-combined CHOP.

Table 5. Multivariate Cox proportional hazard analysis for SIL-2R and categorized IPI in both treatment groups

	Variable	HR	95% CI	*P* value
CHOP				
EFS	SIL-2R			
	Low	1.00		
	High	2.98	1.22–7.29	0.01
	IPI			
	L/L-I	1.00		
	H/H-I	2.47	1.11–5.47	0.02
OS	SIL-2R			
	Low	1.00		
	High	3.12	0.93–10.41	0.06
	IPI			
	L/L-I	1.00		
	H/H-I	4.66	1.60–13.58	0.005
RCHOP				
EFS	SIL-2R			
	Low	1.00		
	High	3.00	1.12–8.07	0.02
	IPI			
	L/L-I	1.00		
	H/H-I	2.06	0.93–4.57	0.07
OS	SIL-2R			
	Low	1.00		
	High	4.30	0.85–21.91	0.07
	IPI			
	L/L-I	1.00		
	H/H-I	4.16	0.80–6.69	0.08

SIL2R, soluble interleukin-2 receptor; IPI, International Prognostic Index; CHOP, cyclophosphamide, doxorubicin, vincristine and prednisone; HR, hazard ratio; CI, confidential interval; EFS, event-free survival; OS, overall survival; LDH, lactate dehydrogenase; RCHOP, rituximab-combined CHOP; L/L-I, low or low-intermediate; H/H-I, high or high-intermediate.

overexpression [24]. BCL6, a marker of germinal center derivation, has been identified as an indicator of favorable outcome in DLBCL [20], although outcome in patients receiving immunochemotherapy was reported to be uninfluenced by BCL6 status [22]. Similarly, no correlation between immunohistochemically defined GC phenotype and survival rate was observed in patients receiving immunochemotherapy [21], in contrast to previous findings of inferior outcomes in non-GC patients relative to GC patients in the prerituximab era [23]. Up to now, no marker other than IPI has been found to be of prognostic relevance since the clinical introduction of rituximab.

The mechanism by which rituximab added to chemotherapy improves outcome in relation to biological features has been evaluated in several studies. They showed that rituximab may suppress the constitutively active nuclear factor-kappa B pathway in non-GC phenotype DLBCL or downregulate Bcl-2-related antiapoptotic proteins, thereby increasing the sensitivity of lymphoma cells to chemotherapy [27–29]. These effects of rituximab may reduce the prognostic significance of the non-GC phenotype and BCL2. Although the mechanism by which SIL-2R retains its prognostic value after addition of rituximab to chemotherapy is unknown, SIL-2R may directly represent the tumor burden [7, 8].

To date, several studies including the present one have demonstrated that IPI score remains predictive in the rituximab era, in contrast to biomarkers [18, 22, 23]. In the present study, the IPI system identified only two risk groups instead of four among our patients—a low and low-intermediate group and a high and high-intermediate group—as reported in previous studies [22, 23].

The addition of rituximab to chemotherapy has improved the outcome of patients. We and others have shown that OS now exceeds 50% even in the groups with unfavorable indicators [14–18, 22, 23], although some patients still have a very poor outcome. Therefore, other predictive factors must be characterized in order to identify patients who should receive alternative initial therapy. A number of molecular prognostic markers have already been identified in patients with DLBCL [30]. These markers now need to be reevaluated in the rituximab era to identify patients with unfavorable prognostic factors and to devise adequate treatment strategies.

In conclusion, we have demonstrated that a high serum SIL-2R level is an indicator of poor prognosis in DLBCL patients receiving rituximab combination chemotherapy. To accurately confirm whether serum SIL-2R influences the outcome of patients receiving rituximab combination chemotherapy, prospective investigation with long-term follow-up will be required.

acknowledgements

The authors are grateful to the members of the Ganken Adult Lymphoma Study Group, including Makoto Kodaira, Shuhei Yamada, Kyoko Ueda and Tomohiro Myojo, for treating the patients at the Cancer Institute Hospital and to Daigo Shoji, Chie Watanabe, Chizuru Suitsu, Ayako Nishito and Michiko Ennishi for collecting the clinical data. Contributions: DE designed the study, treated the patients, collected clinical data and wrote the paper; KT scored the immunohistochemical staining, designed the study and wrote the paper; MY assisted in designing the study and writing the paper; HA treated the patients and collected clinical data; SS, YM, YT and ST treated the patients and assisted in writing the paper; HK, KI and MT supervised the paper and KH designed the study, supervised all aspects of the research and analyses and wrote the paper. Conflict of interest disclosure: The authors declare no competing financial interests.

references

1. Jaffe ES, Harris NL, Stein H, Vardiman JW (eds): World Health Organization Classification of Tumours. Pathology and Genetics of Tumours of Haematopoietic and Lymphoid Tissue. IARC press 2001.
2. TIN-HsLPF. A predictive model for aggressive non-Hodgkin's lymphoma. The International Non-Hodgkin's Lymphoma Prognostic Factors Project. N Engl J Med 1993; 329: 987–994.
3. Gause A, Jung W, Schmits R et al. Soluble CD8, CD25 and CD30 antigens as prognostic markers in patients with untreated Hodgkin's lymphoma. Ann Oncol 1992; 3 (Suppl 4): 49–52.
4. Chilosi M, Semenzato G, Cetto G et al. Soluble interleukin-2 receptors in the sera of patients with hairy cell leukemia: relationship with the effect of recombinant alpha-interferon therapy on clinical parameters and natural killer in vitro activity. Blood 1987; 70: 1530–1535.
5. Wagner DK, Kiwanuka J, Edwards BK et al. Soluble interleukin-2 receptor levels in patients with undifferentiated and lymphoblastic lymphomas: correlation with survival. J Clin Oncol 1987; 5: 1262–1274.
6. Kamihira S, Atogami S, Sohda H et al. Significance of soluble interleukin-2 receptor levels for evaluation of the progression of adult T-cell leukemia. Cancer 1994; 73: 2753–2758.
7. Niitsu N, Iijima K, Chizuka A. A high serum-soluble interleukin-2 receptor level is associated with a poor outcome of aggressive non-Hodgkin's lymphoma. Eur J Haematol 2001; 66: 24–30.
8. Nakase K, Tsuji K, Tamaki S et al. Elevated levels of soluble interleukin-2 receptor in serum of patients with hematological or non-hematological malignancies. Cancer Detect Prev 2005; 29: 256–259.
9. Takeshita T, Asao H, Ohtani K et al. Cloning of the gamma chain of the human IL-2 receptor. Science 1992; 257: 379–382.
10. Rubin LA, Nelson DL. The soluble interleukin-2 receptor: biology, function, and clinical application. Ann Intern Med 1990; 113: 619–627.
11. Smith KA. Interleukin-2: inception, impact, and implications. Science 1988; 240: 1169–1176.
12. Voss SD, Sondel PM, Robb RJ. Characterization of the interleukin 2 receptors (IL-2R) expressed on human natural killer cells activated in vivo by IL-2: association of the p64 IL-2R gamma chain with the IL-2R beta chain in functional intermediate-affinity IL-2R. J Exp Med 1992; 176: 531–541.
13. Fisher RI, Gaynor ER, Dahlberg S et al. Comparison of a standard regimen (CHOP) with three intensive chemotherapy regimens for advanced non-Hodgkin's lymphoma. N Engl J Med 1993; 328: 1002–1006.
14. Coiffier B, Lepage E, Briere J et al. CHOP chemotherapy plus rituximab compared with CHOP alone in elderly patients with diffuse large-B-cell lymphoma. N Engl J Med 2002; 346: 235–242.
15. Habermann TM, Weller EA, Morrison VA et al. Rituximab-CHOP versus CHOP alone or with maintenance rituximab in older patients with diffuse large B-cell lymphoma. J Clin Oncol 2006; 24: 3121–3127.
16. Pfreundschuh M, Trumper L, Osterborg A et al. CHOP-like chemotherapy plus rituximab versus CHOP-like chemotherapy alone in young patients with good-prognosis diffuse large-B-cell lymphoma: a randomised controlled trial by the MabThera International Trial (MInT) Group. Lancet Oncol 2006; 7: 379–391.
17. Sehn LH, Donaldson J, Chhanabhai M et al. Introduction of combined CHOP plus rituximab therapy dramatically improved outcome of diffuse large B-cell lymphoma in British Columbia. J Clin Oncol 2005; 23: 5027–5033.
18. Sehn LH, Berry B, Chhanabhai M et al. The revised International Prognostic Index (R-IPI) is a better predictor of outcome than the standard IPI for patients with diffuse large B-cell lymphoma treated with R-CHOP. Blood 2007; 109: 1857–1861.
19. Gascoyne RD, Adomat SA, Krajewski S et al. Prognostic significance of Bcl-2 protein expression and Bcl-2 gene rearrangement in diffuse aggressive non-Hodgkin's lymphoma. Blood 1997; 90: 244–251.
20. Barrans SL, O'Connor SJ, Evans PA et al. Rearrangement of the BCL6 locus at 3q27 is an independent poor prognostic factor in nodal diffuse large B-cell lymphoma. Br J Haematol 2002; 117: 322–332.
21. Hans CP, Weisenburger DD, Greiner TC et al. Confirmation of the molecular classification of diffuse large B-cell lymphoma by immunohistochemistry using a tissue microarray. Blood 2004; 103: 275–282.
22. Winter JN, Weller EA, Horning SJ et al. Prognostic significance of Bcl-6 protein expression in DLBCL treated with CHOP or R-CHOP: a prospective correlative study. Blood 2006; 107: 4207–4213.
23. Nyman H, Adde M, Karjalainen-Lindsberg ML et al. Prognostic impact of immunohistochemically defined germinal center phenotype in diffuse large B-cell lymphoma patients treated with immunochemotherapy. Blood 2007; 109: 4930–4935.
24. Wilson H, Pittaluga S, O'Connor P. Rituximab may overcome Bcl-2-associated chemotherapy resistance in untreated diffuse large B-cell lymphomas [abstract]. Blood 2001; 98: 343a.
25. Cheson BD, Horning SJ, Coiffier B et al. Report of an international workshop to standardize response criteria for non-Hodgkin's lymphomas. NCI Sponsored International Working Group. J Clin Oncol 1999; 17: 1244.